Time averaging and emerging nonergodicity upon resetting of fractional Brownian motion and heterogeneous diffusion processes

Wei Wang [1,*] Andrey G. Cherstvy [2,3,†] Holger Kantz,[1,‡] Ralf Metzler [2,§] and Igor M. Sokolov [3,4,‖]
[1]*Max Planck Institute for the Physics of Complex Systems, Nöthnitzer Straße 38, 01187 Dresden, Germany*
[2]*Institute for Physics & Astronomy University of Potsdam, Karl-Liebknecht-Straße 24/25, 14476 Potsdam-Golm, Germany*
[3]*Institut für Physik, Humboldt-Universität zu Berlin, Newtonstraße 15, 12489 Berlin, Germany*
[4]*IRIS Adlershof, Zum Großen Windkanal 6, 12489 Berlin, Germany*

(Received 27 April 2021; revised 12 June 2021; accepted 14 July 2021; published 5 August 2021)

How different are the results of constant-rate resetting of anomalous-diffusion processes in terms of their ensemble-averaged versus time-averaged mean-squared displacements (MSDs versus TAMSDs) and how does stochastic resetting impact nonergodicity? We examine, both analytically and by simulations, the implications of resetting on the MSD- and TAMSD-based spreading dynamics of particles executing fractional Brownian motion (FBM) with a long-time memory, heterogeneous diffusion processes (HDPs) with a power-law space-dependent diffusivity $D(x) = D_0|x|^\gamma$ and their "combined" process of HDP-FBM. We find, *inter alia*, that the resetting dynamics of originally ergodic FBM for superdiffusive Hurst exponents develops disparities in scaling and magnitudes of the MSDs and mean TAMSDs indicating weak ergodicity breaking. For subdiffusive HDPs we also quantify the nonequivalence of the MSD and TAMSD and observe a new trimodal form of the probability density function. For reset FBM, HDPs and HDP-FBM we compute analytically and verify by simulations the short-time MSD and TAMSD asymptotes and long-time plateaus reminiscent of those for processes under confinement. We show that certain characteristics of these reset processes are functionally similar despite a different stochastic nature of their nonreset variants. Importantly, we discover nonmonotonicity of the ergodicity-breaking parameter EB as a function of the resetting rate r. For all reset processes studied we unveil a pronounced resetting-induced nonergodicity with a maximum of EB at intermediate r and EB$\sim(1/r)$-decay at large r. Alongside the emerging MSD-versus-TAMSD disparity, this r-dependence of EB can be an experimentally testable prediction. We conclude by discussing some implications to experimental systems featuring resetting dynamics.

DOI: 10.1103/PhysRevE.104.024105

I. INTRODUCTION

A. Overview of recent developments

Resetting a stochastic process, either normal or anomalous [1–10], via restart events—abrupt or taking a finite time, stochastic or random but distributed, or entirely deterministic in time—returns the particle to its initial position (or a set of those) according to a certain rule. In recent years, the field of resetting has experienced a wave of new theoretical developments [11–78] as well as some experimental progress [66,67]. There bouncing-back, often rare, restart events might obey different distributions of waiting times, take place in space-dependent and space-time coupled manner, with power-law time-varying reset rates, with offset-position-dependent probabilities, with varying or stochastic reset jumps, in different geometries and dimensions, in network- and comb-like structures, in confining potentials and under constraints, in nonexponential reset protocols, with interactions (in coagulation-diffusion and reaction-diffusion protocols), for over- and underdamped dynamics, to mention some recent directions of resetting studies.

In most studies, resetting is considered for classical paradigmatic Brownian motion (BM), while resetting studies for more sophisticated fractional- and anomalous-diffusion processes, including continuous-time random walks (CTRWs) and Lévy motion, are less common. Certain first-passage-based, search-related, and search-optimization-like problems involve position restart, with one of the most known manifestations being the minimization of the mean first-passage time to a target at intermediate rates of resetting. A relevant recent study is the first-passage-analysis of a particle in a linear potential with a power-law position-dependent diffusivity, $D(x) \sim |x|$ [61]. Note also that for resetting rates varying in time the nonequilibrium stationary state (NESS) [25,79] was shown [34] to exist for a decay of $r(t)$ slower than $\sim 1/t$. A stochastic velocity reversion for run-and-tumble particles was also considered [40].

B. Some examples of resetting

The list of real-world processes epitomizing resetting or restarting includes, but is not limited to, optimization of some

*weiwangnuaa@gmail.com
†a.cherstvy@gmail.com
‡kantz@pks.mpg.de
§rmetzler@uni-potsdam.de
‖igor.sokolov@physik.hu-berlin.de

 ©2021 American Physical Society

foraging or search strategies [80–87] (employed by animals, fish, insects, microorganisms, bacteria, immune T-cells, etc.) and in behavioral biology [88] (e.g., by a diffusion process with two distinct modes: with a detailed local search and rapid relocations between "patches" likely to yield food) [89–91], relocation of animals to previously frequently visited places [20] and movement-ecology data [20,92–96] in *macro-biological sciences*.

Some examples from the *nano- and microbiological* world are the events of stochastic resetting due to backtracking interrupting a processive motion of RNA polymerase along DNA upon transcription [33] and an alternating switching between the 3D diffusion-based spreading and 1D recognition-based target search in motion of DNA-binding proteins [97–101]. On the level of *simple organisms*, stochastic-switching mechanisms between different phenotypes can be mentioned (employed by various bacteria and fungi to optimize adaptation of a phenotypically diverse population of individuals to fluctuating (and, often, irregularly changing) environments [102–107]).

In *computer* sciences, resetting is involved in strategies for boosting combinatorial-search algorithms [108–110] [via adding a controlled amount of randomization (complete backtracks) to minimize the cumulative search time for a set of tasks or make mean search-times more predictable], and dependency-directed backtracking algorithms in hard constraint-satisfaction problems involving artificial intelligence [108].

Resetting concepts in *psychology* emerge in visual pattern recognition, picture-viewing-, and visual-search-strategies [111–115] (where large-visual-angle jerkinglike saccadic motions are interrupted by fixational tremor-like, jiggling microsaccadic "observational" motions (depending, *inter alia*, on the actual task being posed, the contextual information, habituation effects, etc.) [116–121] and in optimized eye-movement strategies for visual-search tasks (such as in saccadic models of preferred image-search directions maximizing information about the "target") [115,122].

In quantitative *financial mathematics*, the models of option pricing for barrier-type and reset-type options (involving option-price adjustments upon crossing certain price boundaries or at preset dates) are known for decades [123–127]. Abrupt drops of stock-market prices at times of economic crashes and other sudden catastrophic events [60] can also be viewed as reset-related phenomena.

Recent experimental particle-tracking and resetting setups involve a manipulation of micron-sized beads in optical traps [128] and "tweezers" [66,67] and can potentially yield time series amenable for a single-trajectory-based time-averaging analysis aimed at deciphering the underlying diffusion process, as in the theory developed below.

From the theoretical perspective, the diffusive spread of a stochastic process is in a way "confined" by resetting events yielding in the long-time limit a NESS. In this state, the probability-density function (PDF) is quasistationary, but the system still features probability fluxes due to perpetual resetting events of positions of the particles [14]. The main focus of theoretical and simulations-based investigations of resetting in various stochastic processes *so far* was often on the shapes of the PDF (in the NESS and in the particle-displacement phase), scaling relations and plateaus for the mean-squared displacement (MSD), as well as certain first-passage-time-, search-, and surface-adsorption-related quantities.

C. Resetting of SBM: Recent results

Recently, the effects of resetting on the behavior of the MSD and PDF of scaled BM (SBM) [7–9,129–137] with a power-law-like time-dependent diffusion coefficient,

$$D(t) = \alpha K_\alpha t^{\alpha-1} \sim t^{\alpha-1}, \tag{1}$$

with $\alpha > 0$, was considered both for exponential and power-law distributions of waiting times between two consecutive resetting events. We refer the reader here to the two extensive (mainly MSD- and PDF-focused) studies [53,54]. Both nonrenewal (or partial) resetting setups (with resetting of the position only, while keeping the value and the time-variation of the diffusivity unaltered) [53] and renewal (complete resetting of particle position and diffusivity) [54] setups for the SBM diffusivity $D(t)$ in Eq. (1) were considered.

For nonrenewal exponential resetting of single-particle diffusion with the waiting-time distribution

$$\psi(t) = re^{-rt} \tag{2}$$

(a Poissonian precess with a constant rate r and exponential PDF of waiting times between randomly occurring resetting events), the MSD of reset SBM in the limit of strong resetting and long times, at

$$rt \gg 1, \tag{3}$$

was shown to be [53,54]

$$\langle x^2(t)\rangle \approx 2\alpha K_\alpha t^{\alpha-1}/r. \tag{4}$$

So, the MSD of reset SBM acquires an exponent by one smaller than that of conventional or nonreset SBM, with

$$\langle x^2(t)\rangle = \int x^2 P(x,t)dx = 2K_\alpha t^\alpha \tag{5}$$

and PDF

$$P(x,t) = \exp\left[-\frac{x^2}{4K_\alpha t^\alpha}\right]/\sqrt{4\pi K_\alpha t^\alpha}. \tag{6}$$

Here K_α is the generalized diffusion coefficient (with the physical units $[K_\alpha] = \mathrm{m}^2/\mathrm{s}^\alpha$) and α is the anomalous scaling exponent [3,4,8]. Therefore, resetting leaves SBM with $\alpha > 2$ superdiffusive, while superdiffusive SBM with $1 < \alpha < 2$ is being converted after resetting into a process with a subdiffusive growth of the MSD, and, last, initially subdiffusive SBM with $0 < \alpha < 1$ gets totally localized by resetting (all particles are accumulated near the origin at long times).[1]

[1]For a power-law-like (non-Poissonian) nonrenewal resetting, with $\psi(t) = (\beta/\tau_0)/(1 + t/\tau_0)^{1+\beta}$ and $\beta > 0$, it was shown [53,54] that the MSD for reset SBM keeps the exponent of basal SBM and gets only reduced in magnitude for $0 < \beta < 1$. In the range $\beta > 2$ the scaling exponent of the MSD of SBM with resetting gets reduced by one, similarly to the case of exponential or Poissonian resetting in Eq. (4), so that [53,54] $\langle x^2(t)\rangle = 2\alpha\tau_0 K_\alpha t^{\alpha-1}/(\beta-2)$.

For renewal resetting (when both the particle position and diffusivity are being reset), for SBM with exponential resetting the MSD was shown to approach a NESS plateau (denoted by index "pl" below) with the saturation level at [53,54]

$$\langle x^2_{\rm pl}\rangle = 2\,K_\alpha\Gamma(1+\alpha)/r^\alpha. \tag{7}$$

This turns into the known result for BM with exponential constant-rate resetting, namely,

$$\langle x^2_{\rm pl}\rangle = 2\,K_1/r, \tag{8}$$

where $\Gamma(y)$ is the Euler-Legendre Gamma function.[2,3]

D. Outline of the paper

Our main objective here is to enrich the list of important physical observables employed in resetting-dynamics studies by a single-trajectory-based time-averaged MSD (TAMSD) and the ergodicity-breaking parameter EB [see Eqs. (9) and (11) below]. The TAMSD is a quantifier often implemented in single-particle-tracking experiments and its characteristic features have been intensely developed theoretically over the past years for a variety of nonreset stochastic processes featuring anomalous diffusion [8]. The EB parameter characterizes the spread of individual TAMSDs and describes the degree of nonergodicity [8].

The primary focus of this study is on the effects of resetting onto the TAMSD characteristics for stochastic processes of nearly ergodic (see Refs. [138–141]) fractional BM (FBM) [42,142–150] and of nonergodic heterogeneous diffusion processes (HDPs) [132,149,151–155] as well as for a combination of FBM with varying Hurst exponent H [156,157] and HDPs with varying exponent of the power-law-like diffusivity γ [155]. Note that a "hybrid" process of SBM-HDP was also introduced [132] and recently applied to the experimental data [158]. The implications of resetting onto the MSD and PDF of FBM, HDPs, and HDP-FBM are also considered, being a secondary focus.[4]

The paper is structured as follows. We define the observables and present the details of the simulation scheme in Sec. II. In Secs. III, IV, and V—all being similar in presentation style and structure of subsections—we examine the implications of resetting onto the MSD (respective subsections A), PDF (B), TAMSD (C), and EB (D) of reset FBM, reset HDPs, and reset HDP-FBM, correspondingly, as obtained theoretically and from stochastic computer simulations. The features of reset FBM and reset HDPs are compared to those for reset SBM outlined in Sec. I C. The main scaling relations for all three reset processes considered are summarized in Table I. We thus start from the known results for reset SBM in Sec. I C, move to reset FBM (examined now in terms of the MSD, PDF, TAMSD, and EB) featuring some commonalities with reset SBM, and, last, enter the complete *terra incognita* of reset HDPs and reset HDP-FBM, again, examined these reset stochastic processes with the standard measures (MSD and PDF) and novel quantifiers (TAMSD and EB parameter). Finally, we draw conclusions and discuss some applications of our results in Sec. VI. Some supplementary derivations are outlined in Appendices A, B, and C, a number of auxiliary plots are presented in Appendix D, while the abbreviations are listed in Appendix E.

II. OBSERVABLES, MODELS, AND SIMULATION SCHEME

A. Definitions of physical observables

We employ the concept of single-trajectory-based averaging along the time series of particle positions $x(t)$ in terms of the TAMSD [8]

$$\overline{\delta^2(\Delta)} = \frac{1}{T-\Delta}\int_0^{T-\Delta}[x(t+\Delta)-x(t)]^2dt. \tag{9}$$

Here, Δ is the so-called lag time and T is the total length of the time series. After averaging over N statistically independent TAMSD realizations, the mean TAMSD is computed as the arithmetic mean,

$$\langle\overline{\delta^2(\Delta)}\rangle = \frac{1}{N}\sum_{i=1}^{N}\overline{\delta^2_i(\Delta)}. \tag{10}$$

The angular brackets denote hereafter averaging over realizations of noise, while averaging over time is denoted by the overline. To quantify the degree of ergodicity, the so-called ergodicity-breaking parameter EB is utilized [8,145,159]

$$\mathrm{EB}(\Delta) = \langle(\overline{\delta^2(\Delta)})^2\rangle/\langle\overline{\delta^2(\Delta)}\rangle^2 - 1 = \langle\xi^2(\Delta)\rangle - 1, \tag{11}$$

where the dimensionless variable

$$\xi(\Delta) = \overline{\delta^2(\Delta)}/\langle\overline{\delta^2(\Delta)}\rangle \tag{12}$$

[2]For a power-law resetting with $0<\beta<1$, in contrast, the MSD of reset SBM keeps the scaling exponent of free SBM, while the MSD magnitude gets altered by a factor containing the waiting-time PDF exponent β [53,54], $\langle x^2(t)\rangle = 2\,K_\alpha t^\alpha \times \Gamma(\alpha-\beta+1)/[\Gamma(\alpha+1)\Gamma(1-\beta)]$. The MSD behavior differs dramatically for scaling exponents $1<\beta<2$, namely, at long times for $\beta<\alpha+1$ the MSD scales as $\langle x^2(t)\rangle \sim t^{\alpha+1-\beta}$, while for $\beta>\alpha+1$ the MSD approaches a long-time plateau with α- and β-dependent values.

[3]For CTRWs, a similar type of the MSD- and PDF-based analysis for complete resetting (of both particle positions and waiting times) and in the case of partial resetting (of particle positions only) was executed as well [55]. For complete resetting, for CTRWs the behaviors of the MSD and PDF were shown to be the same as for the corresponding SBM. This is expected because SBM is known to be the mean-field model of CTRWs [130].

[4]Note that despite identical PDFs of particle displacements governing SBM and FBM, SBM is a memoryless Markovian process featuring nonstationary increments and nonequivalence of the MSD and TAMSD [134] (often also indicative of weak ergodicity breaking), whereas, in contrast to SBM, FBM is an innately non-Markovian process with a long-time memory and stationary displacement increments, for which the MSD and mean TAMSD are [statistically] equivalent (it is considered as an ergodic process in this sense [8,145,149]). The standard quantifier of ergodicity—the ergodicity-breaking parameter denoted as EB in Eq. (11)—behaves for SBM and FBM, however, rather similarly in terms of EB approach to zero at $\Delta/T \ll 1$. Generally, the stationarity of increments of a stochastic process is a prerequisite of its ergodicity.

TABLE I. Collection of the main asymptotic results for the MSD and mean TAMSD of reset FBM, HDPs, and HDP-FBM, both at short and long times. The conclusions regarding the nonequivalence of both averages (at short times) are listed in the last column.

Stochastic process	MSD and TAMSD	Short-time scaling	Long-time scaling	MSD ≠TAMSD at short times
Reset FBM, $0 < H < 1/2$	$\langle x^2(t)\rangle$	$\sim t^{2H}$, Eq. (23)	$\langle x^2_{\rm pl}\rangle \sim r^{-2H}$, Eq. (25)	No
	$\langle\overline{\delta^2(\Delta)}\rangle$	$\sim\Delta^{2H}$, Eq. (30)	$\langle\overline{\delta^2_{\rm pl}}\rangle \approx 2\langle x^2_{\rm pl}\rangle$, Eq. (32)	
Reset FBM, $1/2 < H < 1$	$\langle x^2(t)\rangle$	Same as for $H < 1/2$	Same as for $H < 1/2$	Yes
	$\langle\overline{\delta^2(\Delta)}\rangle$	$\sim\Delta^1$, Eq. (31)	Same as for $H < 1/2$	
Reset HDPs, $p = \frac{2}{2-\gamma}$	$\langle x^2(t)\rangle$	$\sim t^p$, Eq. (39)	$\langle x^2_{\rm pl}\rangle \sim r^{-p}$, Eq. (42)	Yes
	$\langle\overline{\delta^2(\Delta)}\rangle$	$\sim\Delta^1$, Eq. (47)	$\langle\overline{\delta^2_{\rm pl}}\rangle \approx 2\langle x^2_{\rm pl}\rangle$, Eq. (46)	
Reset HDP-FBM, $0 < H < 1/2$	$\langle x^2(t)\rangle$	$\sim t^{2Hp}$, Eq. (49)	$\langle x^2_{\rm pl}\rangle \sim r^{-2Hp}$, Eq. (50)	Yes
	$\langle\overline{\delta^2(\Delta)}\rangle$	$\sim\Delta^{2H}$, Eq. (55)	$\langle\overline{\delta^2_{\rm pl}}\rangle \approx 2\langle x^2_{\rm pl}\rangle$, Eq. (58)	
Reset HDP-FBM, $1/2 < H < 1$	$\langle x^2(t)\rangle$	Same as for $H < 1/2$	Same as for $H < 1/2$	Yes
	$\langle\overline{\delta^2(\Delta)}\rangle$	$\sim\Delta^1$, Eq. (56)	Same as for $H < 1/2$	

describes the dispersion of individual TAMSD realizations around their mean (10). The distribution of TAMSDs for an ensemble of particle trajectories is characterized by the PDF $\phi(\xi)$ [8,149]. For ergodic BM, the EB parameter in the limit of short lag times and long trajectories, at $(\Delta/T) \ll 1$, vanishes linearly following

$$\mathrm{EB}(\Delta) \approx 4\Delta/(3T). \tag{13}$$

B. Diffusion models

We employ the same simulation scheme as in the recent numerical and analytical investigation of the "compound" process of HDP-FBM introduced in Ref. [155]. Shortly, the overdamped Langevin equation

$$dx(t)/dt = \eta_H(t) \tag{14}$$

with fractional Gaussian zero-mean noise $\eta_H(t)$ featuring the power-law correlation function (for $t \neq t'$),

$$\langle\eta_H(t)\eta_H(t')\rangle \simeq K_{2H} \times 2H(2H-1) \times |t-t'|^{2(H-1)}, \tag{15}$$

is used to simulate free [142,143] and reset FBM in terms of single-particle diffusion.

For HDPs, the same Langevin equation for a zero-mass particle,

$$dx(t)/dt = \sqrt{2D(x)}\eta(t), \tag{16}$$

is modeled with white Gaussian noise having zero mean and unit variance,

$$\langle\eta(t)\eta(t')\rangle = \delta(t-t'), \tag{17}$$

and position-dependent diffusion coefficient of a power-law form [151],

$$D(x) = D_0|x|^\gamma. \tag{18}$$

For $\gamma < 0$, to regularize the diverging diffusivity at the origin, $x = 0$, a modified position-dependent diffusion coefficient is used in simulations, namely [151,155]

$$D(x) = D_0 A/(A + x^{-\gamma}), \tag{19}$$

with the factor $A = 10^{-2}$ [acting as a small offset]. For $2 > \gamma > 0$ no problems with diverging diffusivities occur and the form (18) is used directly. The critical point for the diffusivity exponent is at $\gamma = 2$: upon approaching this point the exponential (and not a power-law-like) growth of the MSD is realized [152,160].

For a stochastic process of HDP-FBM we consider analytically and simulate the overdamped Langevin equation (with the constant $\bar{K} = 1$ having physical units $\sqrt{\mathrm{sec}}/\mathrm{m}$)

$$dx(t)/dt = \sqrt{2D(x)}\bar{K}\eta_H(t). \tag{20}$$

We refer the reader to Ref. [155] for the the details of the analytical solutions, the description of the region of parameters of FBM and HDPs amenable for a solution for HDP-FBM.

C. Some applications of FBM and HDPs

The model of FBM was recently applied to rationalize the non-Brownian anomalous dynamics of lipids, cholesterols, and proteins in or on lipid membranes [161–164], the dynamics of G-proteins and G-protein-coupled receptors on plasma membrane [165,166], the diffusion of labeled mRNAs in living bacterial cells [167], anomalous motion of lipid granules in living yeast cells [168], the diffusion of telomeres inside the nuclei of human cancer cells [169,170], the dynamics of chromosomal loci in bacterial cells [171–173], non-Gaussian nonergodic anomalous diffusion of micron-sized beads in mucin-polymer hydrogels [174], tracer dynamics in actin networks [175] (for the particles larger in size than the network mesh-size) [176], heterogeneous intracellular transport of DNA cargo in cancerous cells (with coexisting ergodic and nonergodic but nonaging dynamics) [177], intermittent bulk-surface non-Gaussian aging subdiffusion of anticancer-drug doxorubicin in silica nanoslits [178], both sub- and superdiffusive FBM-like motion of p-granules in early embryos of nematode worms [179], for various target-search problems [180], to mention a few recent examples.

Solutions of the diffusion equation with variable diffusion coefficients go back to Boltzmann [181], while the nonlinear

diffusion equation with the diffusivity being a power law of concentration of the diffusing substance, $D(C) \sim C^{\epsilon}$, with $\epsilon > 0$, was solved by Pattle [182] (see also some recent "reincarnations" [183,184]). Contemporary models of diffusion with space-dependent diffusion coefficients [160,185–192]—with HDPs being a specific example that assumes the functional diffusivity form (18)—can be used to describe the non-Brownian diffusion in crowded, porous, and heterogeneous media [193–210] (such as densely macromolecularly crowded cell cytoplasm), the reduction of a critical "patch size" required for survival of a population in the case of heterogeneous diffusion of its individuals [189], diffusion in heterogeneous comblike and fractal structures [190], escalated polymerization of RNA nucleotides by a spatially confined thermal (and diffusivity) gradient in thermophoresis setups [211], motion of active particles with space-dependent friction in potentials [212], and transient subdiffusion in disordered space-inhomogeneous quantum walks [213]. We also emphasize the recent data-analysis study of anomalous diffusion of a heterogeneous ensemble of endosomes mathematically describable by a process of "heterogeneous FBM" with distributed scaling exponents and exponent-correlated generalized diffusion coefficients, see Ref. [214].

We mention also a class of diffusion models with concentration-dependent power-law-like diffusivity $D(C) \sim C^{\epsilon}$ [183,215], concentration-dependent dispersion in the population dynamics, with a nonlinear dependence of mobility on particle density, $D(\rho) \sim \rho^{\kappa}$ (yielding a migration from more- to less-populated areas) [216–218], as well as similar nonlinear equations [10] for porous-media dynamics [219], nonlinear heat-conductance systems (with a power-law-like temperature-dependent conductivity), and the dynamics of granular materials [219,220].

D. Algorithm of numerical simulation

We use below the exact theoretical results and asymptotic relations of Ref. [155] for FBM, HDPs, and HDP-FBM processes (without re-deriving them here) and employ the middle-point, physically motivated, Stratonovich-convention-based simulation scheme for Eqs. (14), (16), and (20) (see the details of the Itô-Stratonovich conversion employed and Eq. (32) in Ref. [155]). For all these processes at each elementary time-step of $dt = 10^{-2}$ or $dt = 10^{-3}$ in simulations a constant rate of resetting is implemented r, so that resetting probability to the initial position

$$x_{\rm res} = x(0) = 0 \tag{21}$$

is $r \times dt$; see Fig. 1. When simulating reset FBM we always employ Eq. (21), while for reset HDPs and reset HDP-FBM an offset $x_{\rm res} = 0.01$ is used (to avoid stalling of particles at the origin, especially for superdiffusive HDPs).

The waiting-time distribution of resetting events Eq. (2) yields the average resetting time (subscript "res" below)

$$\langle t_{\rm res} \rangle = \int_0^{\infty} t \times r e^{-rt} dt = 1/r. \tag{22}$$

We consider instantaneous resetting or "jumping-to-the-origin" events [consistent with the inertia-free or overdamped dynamics of the particles in their displacement phase (between the events of resetting)]. Other-than-Poissonian distributions of resetting times, noninstantaneous resetting protocols (constant-velocity, etc.), resetting triggered by crossing of certain thresholds, etc., can also be considered and implemented in simulations.

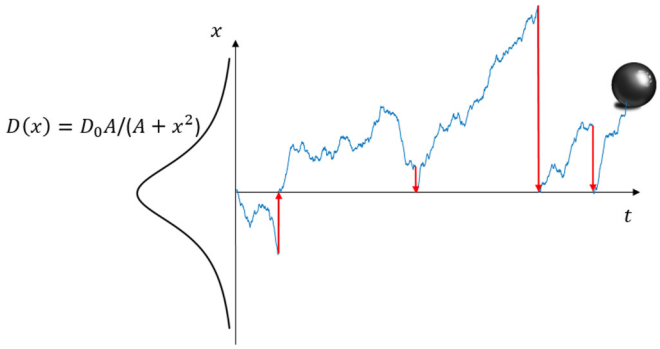

FIG. 1. Simulated trajectory of a subdiffusive HDP with the diffusion-coefficient $D(x) \sim |x|^{-2}$ being shown, in the presence of Poissonian resetting of particles to $x = 0$.

Resetting of FBM, similarly to that of SBM [53,54], can be performed in a partially- or fully-renewal scheme. In the second case, the memory of noise correlations (15) is completely "erased" upon each resetting event: we use this *fully renewal scheme* when simulating exponentially reset FBM and HDP-FBM below. For HDPs, the implementation of resetting is unproblematic because the process is memoryless. In all simulations, we generate particle trajectories for all three reset processes of FBM, HDP, and HDP-FBM via a discretization scheme with a Poissonian-resetting protocol, see Eq. (2). The position $x(t + dt)$ is generated depending on the previous point $x(t)$ via the standard Langevin-dynamics simulation approach [using Eqs. (14), (16), and (20)] when no resetting occurs during the time $t + dt$ (with the probability $1 - r \times dt$) and the particle is moved to the reset position $x_{\rm res}$ (with the probability $r \times dt$) when the resetting event does take place.

III. RESETTING OF FBM

For reset FBM with a fully erased memory—as well as for other Gaussian (Markovian as well as non-Markovian) stochastic processes with the same free-motion PDF as that of SBM—it was predicted (provided after each resetting the particle performs statistically identical diffusion process) to have the same MSD and PDF as for renewal resetting of SBM [54]. In general, one can expect that, both for FBM and HDPs, the events of instantaneous resetting of particle positions to the origin will give rise to *larger* displacements for consecutive time-steps. This not only contributes to a growing magnitude of the TAMSD at short lag times (see below), but also can give rise to a more pronounced irreproducibility of individual TAMSD trajectories and, therefore, larger values of the EB parameter in this region. In the limit of long time, in the NESS the MSD and TAMSD are expected to stagnate and lose any dependence of (lag) time. We substantiate on these intuitive expectations below.

A. MSD

We present the results of analytical computations and findings of computer simulations for the MSD of reset FBM in Fig. 2 (also showing the TAMSD realizations), for several values of the Hurst exponent H, for both sub- and superdiffusive dynamics (in terms of the MSD). For smaller values of H we used a smaller time-step of $dt = 10^{-3}$ to better resolve the short-time behavior of the ensemble- and time-averages. The MSD of FBM with exponential resetting starts unperturbed with the expected short-time behavior characteristic of anomalous diffusion [8,145–147], namely

$$\langle x^2(t)\rangle = 2K_{2H}t^{2H}. \tag{23}$$

At times of the order of the average resetting time (22),

$$t_{\rm pl} \sim (1/r) \times [\Gamma(2H+1)]^{\frac{1}{2H}}, \tag{24}$$

the MSD starts saturating at a plateau (with plateau-related quantities denoted by the subscript "pl" hereafter), with the same height as that for reset SBM [53,54], see Eq. (7). Specifically, for NESS the height of the MSD plateau (with a substitution $\alpha = 2H$) is

$$\langle x^2_{\rm pl}\rangle \approx 2\,K_{2H}\Gamma(2H+1)/r^{2H}, \tag{25}$$

as indicated in Fig. 2. We have checked that this transition behavior for the MSD is the same for the scenarios with and without long-time memory of FBM (15) being included in simulations (results not shown). The consistency of the short-time MSD asymptote (23), the r-dependent MSD plateaus (25), and different onset times onto the NESS-related MSD behavior is demonstrated in Figs. 13 and 14 in Appendix D via presenting the results of computer simulations and the theoretical predictions for several rates of resetting r.

B. PDF

The results for the PDF at intermediate-to-large displacements for reset FBM in the NESS are in full agreement with the predictions for fully reset SBM, given by a time-independent function of the form (with $\alpha = 2H$ to go from SBM- to FBM-expressions) [53,54]

$$P(x) \sim \frac{\sqrt{2}r}{\sqrt{2H(2H+1)}}\left(\frac{2H}{4K_{2H}r}\right)^{\frac{1}{2H+1}}|x|^{\frac{1-2H}{1+2H}} \times \exp\left[-\left(\frac{x^2r^{2H}}{4K_{2H}}\right)^{\frac{1}{2H+1}}\left((2H)^{\frac{1}{2H+1}}+(2H)^{-\frac{2H}{2H+1}}\right)\right]. \tag{26}$$

The leading functional behavior for the PDF "tails" in Eq. (26) is a stretched-or-compressed exponential function [53,54],

$$P(x) \sim \exp\left[-{\rm const}(r,H)\times|x|^{\frac{2}{2H+1}}\right]. \tag{27}$$

We have checked that the levels for the MSD plateaus in the NESS, $\langle x^2_{\rm pl}\rangle$, are well described using the approximate PDF (26), especially for $H \gtrsim 1/2$, as shown in Fig. 16.

In Fig. 3 we present the agreement of the results of computer simulations for the PDF of reset FBM with the theoretically shape (26) at long times in the NESS and for intermediate-to-large displacements of the particles. The

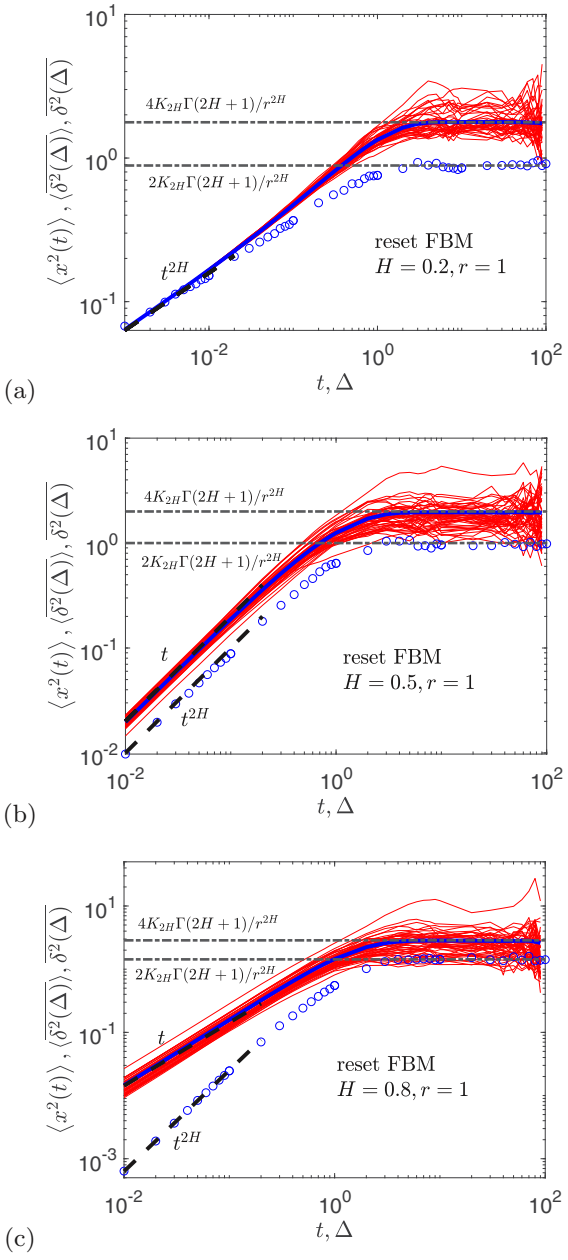

FIG. 2. Magnitude of the MSD (blue circles), the spread of individual TAMSDs (thin red curves), and the mean TAMSD (thick blue curve) for the dynamics of reset FBM (see Fig. 15), shown for varying values of the Hurst exponent (the values of H are indicated in the legends). Simulations of resetting are conducted with no FBM-related memory effects. Theoretical long-time plateaus for the MSD and mean TAMSD are given by Eqs. (25) and (32), respectively. Here and below, all the MSD and mean TAMSD asymptotes are shown in the plots with their exact numerical prefactors being included. The short-time asymptote for the MSD is Eq. (23), while the evolution of the mean TAMSD at short lag times follows Eqs. (30) and (32), for subdiffusive and superdiffusive FBM, correspondingly. The asymptotes are shown as the black dashed and dot-dashed lines. Parameters: the length of the trajectories is $T = 10^2$, the elementary time-step in simulations is $dt = 10^{-2}$ (except for $H = 0.2$ with $dt = 10^{-3}$), the number of trajectories for ensemble averaging is $N = 10^4$, the resetting rate is $r = 1$ (the resetting probability per step is $r \times dt = 10^{-2}$), and the generalized diffusion coefficient is set to $K_{2H} = 1/2$.

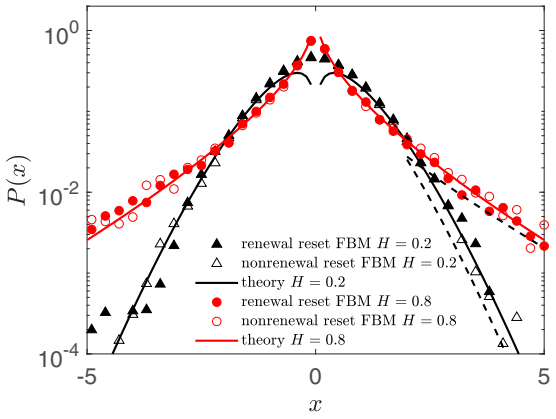

FIG. 3. Shapes of the PDFs of reset FBM, computed for the Hurst exponents $H = 0.2$ with $dt = 10^{-3}$ and $H = 0.8$ with $dt = 10^{-2}$ (see the legend) at $r = 1$. The symbols represent the results of simulations, while the solid curves are the theoretical intermediate-to-long-times expectations for the PDF given by Eq. (26). The dashed lines at large displacements are stretched- or compressed-exponential asymptotes for the PDF tails [53,54] given by Eq. (27).

shapes of the PDF for reset FBM with and without memory are statistically identical at these conditions. We prove this in Fig. 3 presenting the results for sub- and superdiffusive choices of H. Note also that the MSD evolution for reset FBM with and without memory is also identical (results not shown). For resetting rate $r = 1$, the FBM dynamics at $H = 0.8$ is much faster than at $H = 0.2$. For a preset or fixed length of simulated trajectories, the MSD plateaus for reset FBM at $H = 0.8$ occupy a rather extended time domain, while the quasistationary state for a slower dynamics at $H = 0.2$ is not yet realized, compare Figs. 2(c) and 14(b) at $r = 1$.

The PDF shapes for reset FBM evolve upon approaching the NESS. We find that for $r = 1$ the PDF shape at the origin for strongly subdiffusive reset FBM is almost smooth and Gaussian (as for nonreset FBM), while for the same rate of resetting for strongly superdiffusive reset FBM the PDF exhibits a pronounced cusp at the origin stemming from the returning events of the particles. This cusp is well described by the theoretical prediction Eq. (26), see Fig. 3, and it corroborates with the emergence of the NESS plateaus of the MSD and mean TAMSD. The empty and filled symbols in Fig. 3 show the results of reset-FBM simulations with and without the long-time memory of noise being taken into account: in Fig. 3 we check the validity of the theoretical PDF once for nonrenewal resetting of FBM too. Therefore, for considerably larger values of r, when for strongly subdiffusive reset FBM the MSD also reveals a plateau in the NESS (results not shown, but see Fig. 14(c) for the onset on this saturating behavior at $r = 3$), the respective PDF of reset FBM at $H = 0.2$ also has a cusp at $x = 0$, as shown in Fig. 17.

The PDF cusp for subdiffusive reset FBM is not in agreement with Eq. (26) and it critically depends on the simulation time-step. Ideally, the probability of resetting each step should be small in order for the results to be independent on the time-step used in simulations. The numerical integration of the long-time limit of the PDF (B1)—evidently step-size-independent—does not reveal any cusp at $x = 0$, see the cross-symbols in Figs. 17 and 18. As we reduce the simulation time-step from $dt = 0.01$ to 0.001 keeping the resetting rate the same, the PDF peak in simulations for $H = 0.2$ vanishes and the PDF form nicely agrees with the results of numerical integration of Eq. (B1); see Fig. 18. This numerical inaccuracy giving rise to the "spurious" PDF cusp for $H = 0.2$ gives rise to small, but systematically measurable, deviations in the plateau heights of the MSD and mean TAMSD in the NESS for the simulations for very large r (results not shown). Note that for reset SBM [53,54] the PDF shape from the theory was shown as a combination of the results of the Laplace approximation Eq. (26) [valid at intermediate-to-large separations from the origin], while the central PDF part near $x = 0$ was the cusp-free numerical integration of the exact PDF expression (B1).

Note that the approximate Laplace-method-based PDF (26) is generally not normalized: for subdiffusive (superdiffusive) reset FBM it underestimates (overestimates) the integral $\int P(x)dx$, as shown in Fig. 19. We still call this approximate nonnormalized distribution function a PDF hereafter, for brevity. The PDF (26) describes the simulation data well at intermediate-to-large separations [53,54], for $|x| \gtrsim x^\star$. The deviations from the results of computer simulation at small $|x|$ values from Eq. (26) are especially pronounced for very subdiffusive reset FBM. A rough estimation for the threshold separation $x^\star$ for reset FBM with $H < 1/2$ follows [based on the realized PDF shapes] from solving $\partial P(x)/\partial x|_{x=x^\star} = 0$ for the inflection point, that gives

$$x^\star(H, r) = \left(\frac{1/2 - H}{1 + 1/(2H)}\right)^{H+1/2} \left(\frac{2K_{2H}}{Hr^{2H}}\right)^{1/2}, \qquad (28)$$

see the inset of Fig. 19 showing $x^\star(H)$ variations.

The exponential decay of the PDF of reset FBM in the NESS given by Eq. (27) [identical to that of full Eq. (26)] as well as the scaling relation for the growth-dynamics of the NESS domain with time given by $\sim t^{H+1/2}$ were obtained before in Ref. [25]. The NESS starts getting established from the restart position, with the spatial NESS domain growing quicker in time than a typical FBM diffusion length that scales as $\propto \sqrt{\mathrm{MSD}(t)} \sim t^H$. Outside of this PDF- and MSD-stationarity domain, the reset system still performs relaxation and features a time-dependent PDF [describing the trajectories with almost no resetting occurred so far]. In Fig. 20 the PDF decay derived in Ref. [25] is explicitly compared to our simulation data for subdiffusive reset FBM.

To quantify the height of the PDF at the point of particle resetting in the NESS, in Fig. 21 we show the results of computer simulations for the values of $P(x = 0)$ for reset FBM. As for nonreset FBM, the PDF is identical to that of pure SBM [given by Eq. (6)], using the PDF-transformation relation Eq. (B1), for reset FBM in the NESS the PDF at the point of return assumes the value

$$P(x = 0) \approx \int_0^\infty \frac{re^{-r\tau}\tau^{-H}}{\sqrt{4\pi K_{2H}}} d\tau = \frac{r^H \Gamma(1 - H)}{\sqrt{4\pi K_{2H}}} \propto r^H. \qquad (29)$$

The asymptotic long-time law $P(x = 0) \sim r^H$ excellently agrees with the results of our simulations, see Fig. 21.

C. TAMSD

We find from simulations that for subdiffusive Hurst exponents, with $0 < H < 1/2$, the TAMSD starts sublinearly and has roughly the same magnitude as the short-time MSD Eq. (23), namely

$$\langle\overline{\delta^2(\Delta)}\rangle \approx 2K_{2H}\Delta^{2H}. \tag{30}$$

For initially superdiffusive FBMs, in the range of Hurst exponents $1/2 < H < 1$, in contrast, the mean TAMSD is linear at short lag times,

$$\langle\overline{\delta^2(\Delta)}\rangle \approx 2\,K_{2H}\Gamma(2H+1)/r^{2H} \times (r\Delta)^1, \tag{31}$$

as shown in Fig. 2. In Appendix A we provide the derivation of asymptotes (30) and (31). For $H = 1/2$ we need to take the sum of two independent terms (30) and (31) to *quantitatively* fit the short-lag-time behavior of the mean TAMSD.

At long lag times for reset FBM the TAMSD plateau in the NESS is realized, with the magnitude of twice that of the MSD plateau [given by Eq. (25)], namely,

$$\langle\overline{\delta^2_{\rm pl}}\rangle \approx 2 \times 2\,K_{2H}\Gamma(2H+1)/r^{2H}. \tag{32}$$

The ratio

$$\langle\overline{\delta^2_{\rm pl}}\rangle/\langle x^2_{\rm pl}\rangle = 2 \tag{33}$$

in the long-time (quasistationary) limit is known also for FBM confined in harmonic potentials [147] and interval-confined HDPs [153]. This twice-the-MSD magnitude in Eq. (32) stems from the TAMSD definition Eq. (9) and is not related to resetting *per se*. The reason being that after multiple resettings in the NESS the process values at $x(t+\Delta)$ and $x(t)$ become almost independent, so that

$$\langle[x(t+\Delta)-x(t)]^2\rangle \approx \langle x^2(t+\Delta)\rangle + \langle x^2(t)\rangle \approx 2\langle x^2_{\rm pl}\rangle, \tag{34}$$

yielding Eq. (33).

We stress, however, that for FBM in parabolic potentials at short lag times the MSD and mean TAMSD are fully equivalent in magnitude and scaling [147]. This fact is in stark contrast to reset FBM studied here, where weak ergodicity-breaking and MSD-versus-TAMSD nonequivalence emerges at $H > 1/2$, see also Table I. Indeed, we observe that for reset FBM the mean TAMSD in the region of short lag times always increases in magnitude as compared to that of free or nonreset FBM. At the very last point of the trajectory, at $\Delta \to T$, the magnitude of the mean TAMSD approaches that of the MSD in the plateau region. This fact is, however, not very well visible in Figs. 2, 13, and 14 because of a logarithmic sampling of the data (with only ten points per decade).

Via equating the short-lag-time TAMSD asymptotes and the long-time TAMSD plateau one can assess the lag time at which the TAMSD plateau (32) starts to be followed as $\Delta_{\rm pl} \sim (1/r) \times [2\Gamma(2H+1)]^{\frac{1}{2H}}$ for $0 < H < 1/2$ and $\Delta_{\rm pl} \sim 2/r$ for $1/2 < H < 1$. To assess the effects of a varying resetting rate r, in Fig. 13 we present the results of computer simulations for the largest Hurst exponent $H = 0.99$ (when the scatter of individual $\overline{\delta^2(\Delta)}$ trajectories is the broadest [for the same (fixed) r], see also Sec. III D) at varying r values. We observe that the predicted r-dependent plateaus for the MSD and mean TAMSD at long times in the NESS, Eqs. (25) and (32), respectively, excellently describe the results of simulations.

The spread of individual TAMSD realizations for the resetting dynamics of FBM typically increases, as compared to that of free FBM with $\mathrm{EB}(\Delta) \to 0$ for long trajectories and short lag times (at $\Delta/T \to 0$) in the continuous-time formulation (see Refs. [138–140] for the definition(s) and general discussion of ergodicity), as demonstrated in Refs. [8,145,149,150]. This effect is particularly pronounced for large superdiffusive, H, as illustrated in Figs. 2(c) and 13. In the region of resetting rates r considered in Fig. 13 for $H = 0.99$ the relative spread of the TAMSDs increases with decreasing r. Note, however, that the variation of the dispersion of individual TAMSDs as a function of the Hurst exponent and resetting rate is rather nontrivial, as we unveil below.

In contrast, for strongly subdiffusive Hurst exponents, see, e.g., the results presented in Fig. 14 for $H = 0.2$, the impact of the resetting rate [varying in the same interval] is rather weak. This is intuitively clear: as compared to the trajectories of strongly superdiffusive FBM which depart far away from the origin and thus are strongly impacted by a given resetting rate, for very subdiffusive FBM the trajectories are weakly fluctuating in a close proximity of the starting position, so that the impact of events of particle's resetting to zero is nearly unnoticed in our quantifiers. To substantiate on this claim, in Fig. 15 two FBM trajectories for $H = 0.8$ and $H = 0.2$ are presented in the absence and in the presence of resetting.

D. EB

1. Distribution of the TAMSDs

The distribution of TAMSDs for reset FBM at $H = 0.8$ is presented in Fig. 22. We find that for small rate of resetting the distribution $\phi(\xi)$ at short lag times for a weakly reset FBM is considerably skewed toward the region $\xi > 1$. This fact (known not only for FBM [149,151]) stems from the existence of a natural boundary at $\xi = 0$ [as ξ is positively defined, Eq. (12)] and an unbounded domain extending to $\xi \gg 1$. As the rate of resetting increases for FBM with a given H (in the range of r chosen), the TAMSD realizations become progressively less scattered around their mean, indicative of a more reproducible (or ergodic) dynamics in terms of scatter, described by $\phi(\xi)$.

The variation of the EB parameter of reset FBM versus the lag time for several values of H is presented in Fig. 4. We observe that for larger H values the magnitude of EB shifts upwards (and does so not only for short lag times, but also in the entire range of Δ). We also find that $\mathrm{EB} = 2$ is the terminal value at $\Delta = T$. The variation of $\mathrm{EB}(\Delta)$ at the shortest lag time $\Delta = \Delta_1$ with varying H exponent is observed to be the strongest. The region of EB-parameter saturation at intermediate Δ emerges roughly at lag times of the plateau-like behavior of the mean TAMSD corresponding to the NESS. As inferred also from the spread of the TAMSDs—which is roughly lag-time-independent in this region, as shown in Fig. 2—nearly constant and Δ-independent values of EB corroborate these findings. The height of the EB plateaus in this NESS regime and short-lag-time EB values are both H-dependent. The overall $\mathrm{EB}(\Delta)$-variation for reset FBM in

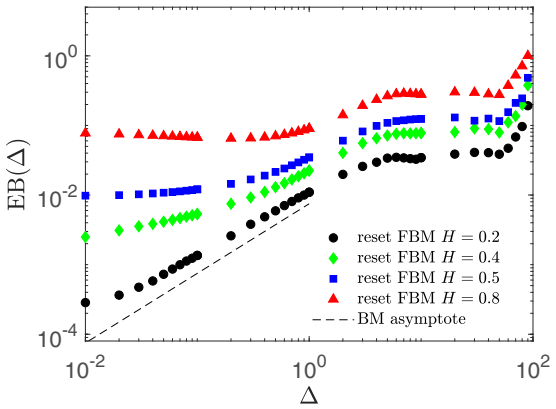

FIG. 4. EB parameter of reset FBM, computed at a fixed resetting rate $r = 1$ and for the trace length $T = 10^2$, plotted versus the lag time Δ for several values of the Hurst exponent (see the legend). The BM-asymptote (13) is the black dashed line at short lag times.

Fig. 4 is similar to that found for the Ornstein-Uhlenbeck process [222] (see Figs. 4 and 5 in Ref. [221]). The protocol of exponential resetting, therefore, acts on the TAMSD and EB similarly as (harmonic) confinement, as one could intuitively expect. The detailed analytical derivation of EB for reset FBM will be presented elsewhere [223].

2. Large r values

This enhanced reproducibility of TAMSD realizations in this range of rates r is also reflected in decreasing values of the EB parameter computed at $\Delta = \Delta_1$, see Fig. 5 for $H = 0.8$. A qualitatively similar behavior of EB versus r is also observed in our computer-simulated data for reset FBM at $H = 0.5$ and 0.4, but in a progressively smaller range of resetting rates, see Fig. 5. At these "intermediate" r values, for reset FBM with elevated Hurst exponents, the value of EB at short lag times

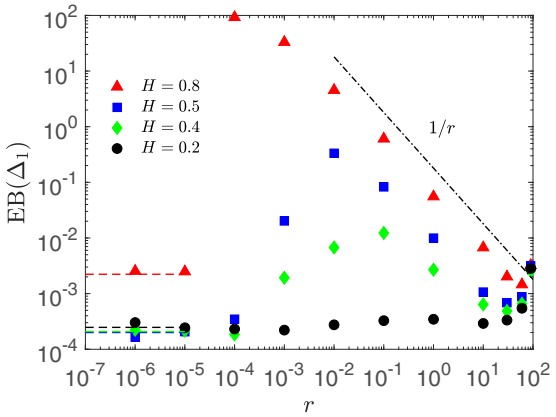

FIG. 5. Dependence of the EB(Δ_1) parameter (11) on the rate of FBM resetting r, computed for $T = 10^2$ at $\Delta_1 = dt = 10^{-2}$, for a set of H exponents. The asymptote (35) is the black dot-dashed line at intermediate-to-large resetting rates. The values of EB for nonreset FBM are the dashed plateaus with the H-respective colors at $r \to 0$ (see the legend).

drops according to

$$\mathrm{EB}(\Delta_1, r) \sim 1/r, \tag{35}$$

and larger Hurst exponents yield larger EB.

Therefore, the dependence (35) of EB(Δ_1, r) on r in this r-range for reset FBM with elevated H is functionally similar to that of EB(Δ_1) on $1/T$ repeatedly detected for a number of (both normal and anomalous) stochastic processes [8]. The latter indicates progressively more ergodic behavior for longer trajectories, so that the relation EB(T, Δ_1) $\sim 1/T$ holds. The decrease of EB values with r (in the limit of frequent resetting) for reset FBM with larger Hurst exponents is corroborated by a shrinking $\phi(\xi(\Delta_1))$ distribution of the TAMSDs computed for the same conditions with increasing r, as shown in Fig. 22. In contrast, for strongly subdiffusive reset FBM we observe a nearly *constant* EB upon varying r, see Fig. 5 for $H = 0.2$.

For strong or frequent resetting, as the probability of a reset event at each displacement step approaches unity, the EB parameter becomes very sensitive to the step-size value [discreteness effects, as those for the PDF cusps at $x \to 0$ in Fig. 18]. For instance, our simulations for $T = 10^2$ with $dt = 10^{-2}$ yield similar intermediate-to-large-r behavior of EB and actual EB values for *superdiffusive* reset FBM as compared to those at $dt = 10^{-3}$ (with 10-times more points per trajectory), see Fig. 23. For smaller time-steps—when even for the largest reset rates studied the condition $r \times dt \ll 1$ is satisfied and the reset probabilities per step are small (the Poissonian statistics still applicable)—the EB-versus-r scaling relation (35) is valid up to $r = 100$, see Fig. 23 (compare to the data of Fig. 5).

We stress here also the essential differences in the behavior and magnitudes of EB from the discrete-time stochastic simulations versus those from a continuous-time theory [145], as studied in Ref. [150]. For instance, for subdiffusive FBM the EB value at a fixed lag time Δ_1 and trajectory length T loses its dependence on Hurst exponent and stagnates at a discretization-induced *plateau*, with the height decreasing with the number of points in the trajectory $\bar{N}$ as [150]

$$\mathrm{EB}_{\mathrm{pl}}(\Delta_1, \bar{N}) \sim 1/\bar{N}. \tag{36}$$

The EB values computed at short lag times for subdiffusive reset FBM scale with the time-step $dt = T/\bar{N}$ used in the simulations. In Figs. 5 and 23 the simulation data for reset FBM presented for two different time-steps illustrate the EB(Δ_1)-variation Eq. (36) with dt, compare the data for $H = 0.2$ at intermediate-to-large r values. To summarize, when simulating the EB parameter for reset-FBM dynamics a special care regarding the time-step chosen is to be taken (especially for large r values) and regarding comparison of the obtained EB values versus the theoretical predictions (especially for small EB values affected by step-size discreteness).

For strongly subdiffusive reset FBM the variation of EB(Δ_1) with r does not exhibit any maximum at intermediate r; see also Ref. [223]. The maximum of EB versus r is realizable, however, for slightly subdiffusive FBM, see Fig. 5 for $H = 0.4$. We also stress that for reset FBM the variation of EB(Δ_1) with resetting rate r stays qualitatively similar also for longer trajectories, with the EB values reduced according

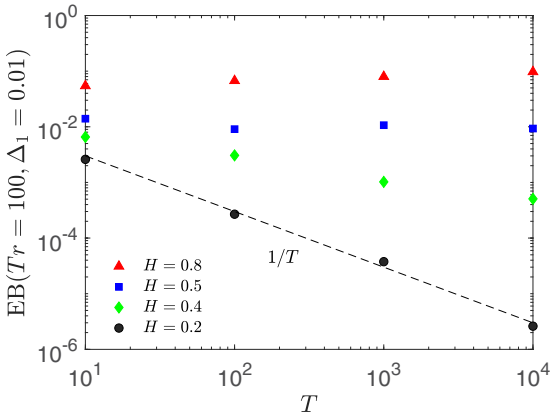

FIG. 6. EB parameter $\mathrm{EB}(\Delta_1, rT)$ of reset FBM for "rescaled" trajectory lengths. EB is computed for *simultaneously* varying r and T such that $rT = \text{const} = 10^2$ (at $dt = \Delta_1 = 10^{-2}$). At $H = 0.8$ and 0.5 the computed EB values are nearly constant, as per Eq. (37), while for $H = 0.2$ EB still decays with T as $\sim 1/T$.

to $\mathrm{EB}(\Delta_1, T) \sim 1/T$ relation (as for free BM [8] and FBM with $0 < H < 3/4$ [145,150]), see Fig. 24.

From the theoretical perspective, as the reciprocal rate of resetting defines a *new time-scale* for the process of reset FBM, r^{-1}, the length of the time series for an appropriate comparison of "relaxation to ergodicity" quantified via respective EB values should be renormalized as

$$T \to T_r \equiv rT. \tag{37}$$

This time-rescaling "scales out" the apparent nonergodicity for strongly superdiffusive reset FBM, having the strongest effects onto EB due to the quickest underlying dynamics. Specifically, when r and T are being varied simultaneously but such that $rT = \text{const}$, for $H \geqslant 0.5$ we find in Fig. 6 that the systematic decay of $\mathrm{EB}(\Delta_1)$ with r given by Eq. (35) in the region

$$\Delta_1 \ll r^{-1} \ll T \tag{38}$$

of frequent resetting turns into a *nearly constant* EB. For smaller values of H—when the region of decay (35) covers a smaller range of r—the expected rescaling (37) holds naturally only for that domain of r and T. When resetting has weak or no effects onto EB at all, as for very subdiffusive reset FBM in Fig. 5, one does not expect time-rescaling (37) to work. Here, one can compare the nearly constant EB values for $H = 0.8$ and the EB values decreasing as $\sim 1/T$ for $H = 0.2$ for a nonreset process, when for both H values r and T are varied such that rT =const, as in Fig. 6.

Note that from the experimental perspective such a rescaling of physical time might not always be easy to implement and the variation of $\mathrm{EB}(\Delta_1, r)$ with r recorded for a *fixed* trajectory length T might be more accessible for the analysis of time series from single-particle-tracking experiments, with the decay law (35) expected for EB of frequently reset FBM; see Ref. [223] for the analytical derivation.

3. Small r values

For very weak or rare resetting, we recover the small values of the EB parameter characteristic for ergodic free FBM [8,145,150] at $\Delta/T \ll 1$ at the corresponding H values, computed recently [155] and denoted as the dashed lines of respective colors in Fig. 5 (in the regime of small r values). We emphasize, however, that the approach of EB of reset FBM to that of nonreset FBM yields a *nonmonotonic dependence* of $\mathrm{EB}(r)$—particularly strong for very superdiffusive, but also present for slightly subdiffusive—reset FBM. This nonmonotonicity of $\mathrm{EB}(\Delta_1)$ yields a strongly resetting-enhanced dispersion of short-lag-time magnitudes of individual TAMSDs of reset FBM at intermediate resetting rates. The maximum of EB as a function of r—characterizing the strongest irreproducibility of TAMSDs—shifts toward smaller r values for more superdiffusive FBMs, compare the data for $\mathrm{EB}(r)$ for $H = \{0.8, 0.5, 0.4\}$ in Fig. 5. We find that the maximally achievable EB values for strongly superdiffusive reset FBM at intermediate r are colossal, about four orders of magnitude larger than the respective EB values for free FBM with the same T [145,150].

IV. RESETTING OF HDPS

A. MSD

At short times, the MSD of reset HDPs starts similarly to that of unperturbed HDPs, as shown in Fig. 7, namely, following the power law

$$\langle x^2(t) \rangle \approx C_p t^p, \tag{39}$$

where the scaling exponent, $p(\gamma)$, is given in terms of the exponent of the space-dependent diffusivity (18) by [151]

$$p = 2/(2 - \gamma), \tag{40}$$

and the prefactor C_p in Eq. (39) is [151]

$$C_p = \Gamma(p + 1/2)\pi^{-1/2}(2/p)^{2p}(D_0)^p. \tag{41}$$

The MSD plateau (see Appendix B for the derivation)

$$\langle x^2_{\mathrm{pl}} \rangle \approx C_p \Gamma(p + 1)/r^p \tag{42}$$

is realized at long times (in the NESS). This expression for the stagnating MSD features the same functional form as the MSD plateau of the reset-FBM process in Eq. (25), with the pair of parameters $\{p, C_p\}$ effectively playing the role of $\{2H, K_{2H}\}$. The typical time at which the MSD plateau of Eq. (42) starts to be followed can be estimated—from equating the growth law (39) and plateau height (42)—as

$$t_{\mathrm{pl}} \sim (1/r) \times [\Gamma(p + 1)]^{\frac{1}{p}} \sim 1/r. \tag{43}$$

B. PDF

The approximate PDF of reset HDPs at intermediate-to-long separations follows from the general consideration for reset HDP-FBM processes (see Appendix C for the derivation, and also Sec. V) at $2H = 1$ as

$$P(x) \approx \frac{1}{2}\sqrt{\frac{r}{D_0}}|x|^{1/p-1} \exp\left[-p\sqrt{\frac{r}{D_0}}|x|^{1/p}\right]. \tag{44}$$

This PDF (truly normalized at $H = 1/2$, see Fig. 19) has a Laplacian-like shape in variable $|x|^{1/p}$ as compared to the Gaussian-like PDF of nonreset HDPs given by expression

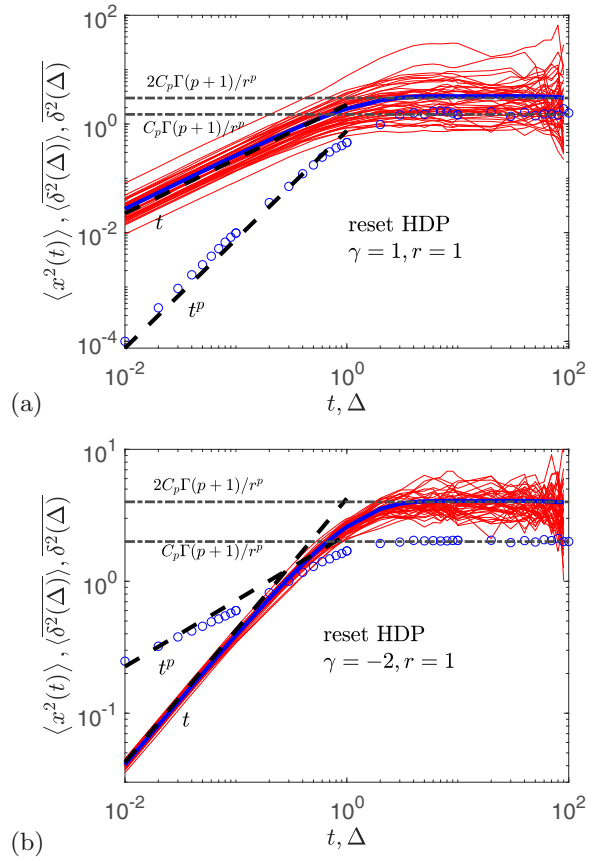

FIG. 7. The same as in Fig. 2, but for reset HDPs, computed for the scaling exponents of $D(x) \sim |x|^\gamma$ being $\gamma = 1$ (a) and $\gamma = -2$ (b), corresponding to super- and subdiffusive HDPs, respectively. The theoretical short-time asymptotes Eqs. (39) and (48) and the NESS-related long-time MSD and mean TAMSD plateaus given by Eqs. (42) and (46), respectively, are the dashed black lines. The magnitude of the diffusivity (18) is fixed in simulations to $D_0 = 1$.

(C1). Additionally, for $p = 1$ it turns into the PDF of canonical reset BM [13,14,25,53,54] given by

$$P(x) = (1/2)\sqrt{r/D_0}\exp(-\sqrt{r/D_0} \times |x|). \tag{45}$$

Note that the PDF form (44) cannot predict trimodality observed in computer simulations for reset HDPs with scaling exponents $\gamma < 0$ because the ideal theoretical consideration yielding the free-HDP PDF Eq. (C1) is based upon assuming *infinite* diffusivity at the origin (that, in turn, instantly relocates the particles from there, so that one expects $P(x = 0) = 0$), while in the *in-silico*-reality of simulations the diffusion coefficient for subdiffusive HDPs has to have finite values at the origin, see Eq. (19), yielding $P(0) \neq 0$. We quantify the physical reasons of trimodality of PDFs and the dependence of PDF heights at the origin for a general scenario of HDP-FBM processes in Sec. V B below.

For reset subdiffusive HDPs ($\gamma < 0$) in the NESS for the trimodal PFD shapes observed in simulations (at certain conditions, see Sec. V B) the two side peaks stem from the spreading dynamics of nonreset HDPs, while the central peak at $x = 0$ emerges due to resetting to the origin, see Fig. 8. The PDFs for reset superdiffusive HDPs, with the diffusivity exponents $2 > \gamma > 0$, have a single peak/cusp at the origin,

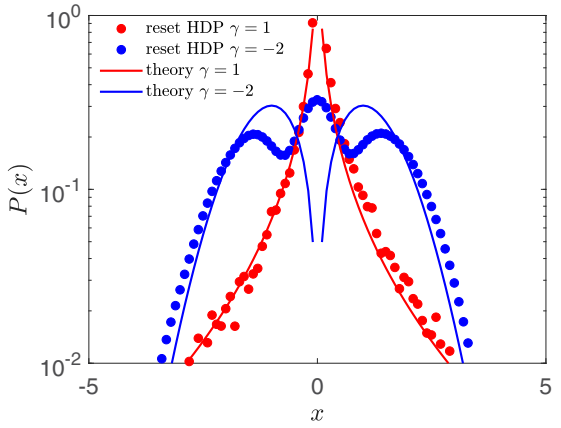

FIG. 8. Shapes of the PDFs of reset HDPs plotted for the same scaling exponents of the diffusivity as in Fig. 7, and at diffusion time $T = 10^2$ in the NESS, as indicated in the legend. The theoretical asymptote of Eq. (44) is the solid curve.

due to the return events and the influx of particles at $x = 0$, leaving the general PDF shape largely unaltered.

C. TAMSD

We start with the long-lag-time behavior here, where a plateau of the mean TAMSD develops, as demonstrated in Fig. 7. The height of this plateau is twice that of the MSD plateau in Eq. (42), namely,

$$\langle\overline{\delta^2_{\rm pl}}\rangle \approx 2 \times \langle x^2_{\rm pl}\rangle \approx 2 \times C_p\Gamma(p+1)/r^p, \tag{46}$$

similar to the TAMSD-versus-MSD plateaus for reset FBM. At short lag times, the linear growth of the mean TAMSD with lag time known for HDPs [151,155],

$$\langle\overline{\delta^2(\Delta)}\rangle = \langle x^2(T)\rangle \times \Delta/T = C_pT^p \times \Delta/T, \tag{47}$$

stays unaltered for reset HDPs, see Fig. 7. Specifically, using the input from computer simulations regarding the linear growth at short lag times and the TAMSD plateau (46) at long lag times, the following approximate evolution of the TAMSD with the lag time can be proposed,

$$\langle\overline{\delta^2(\Delta)}\rangle \approx (1/2)\langle\overline{\delta^2_{\rm pl}}\rangle \times (r\Delta)^1 + C_pr^{-p} \times (r\Delta)^1. \tag{48}$$

The second term in this expression is analogous to that in Eq. (47), with the inverse reset rate playing the role of the trajectory length in the prefactor, i.e., $1/r \leftrightarrow T$.

The spread of individual TAMSD trajectories for subdiffusive reset HDPs becomes relatively small, see Fig. 7(b). It is visible in particular for small scaling exponents γ when the nonreset HDPs are only weakly nonergodic (with the MSD and mean TAMSD being close in magnitude and in values of their scaling exponents). For superdiffusive HDPs with resetting, the spread of individual TAMSDs is comparatively large, see the behaviors of the MSD and mean TAMSD for $\gamma = -2$ and $\gamma = 1$ illustrated in Fig. 7.

D. EB

The degree of irreproducibility of TAMSD realizations and nonergodicity for reset HDPs depends on the sub- ver-

sus superdiffusive nature of nonreset HDPs. In particular for superdiffusive reset HDPs, similarly to the results for superdiffusive reset FBMs in Fig. 5, the EB parameter exhibits a maximum at intermediate rates of reset, see the results shown in Fig. 12 for the case $H = 1/2$. For subdiffusive reset HDPs, the EB parameter reveals a plateau in the limit of rare resetting, $r \to 0$ (with the height not very sensitive to the exponent γ). In the limit of strong resetting, on the other hand, both sub- and superdiffusive HDPs feature EB decreasing rapidly as $\sim 1/r$ with the rate of resetting, as illustrated in Fig. 12. We thoroughly describe the results for $\mathrm{EB}(\Delta_1, r)$ variation with r for a more general process of HDP-FBM in Sec. V D.

As a comparison, for interval-confined nonreset HDPs the spread of TAMSD realizations at short lag times was severely restricted by confinement and the values of the EB parameter were shown to decrease as $\sim 1/T$ with the trajectory length T, even in the very confined scenarios; see Figs. 4, 6(b), and 6(d) in Ref. [153]. We stress that the MSD-TAMSD inter-relation $\langle \overline{\delta^2_{\mathrm{pl}}} \rangle \approx 2\langle x^2_{\mathrm{pl}} \rangle$ was also valid for the interval-confined HDPs in the limit of long times, after multiple "reflections" of the particles from the confining walls took place.

V. RESETTING OF HDP-FBM

A. MSD

The MSD of reset HDP-FBM at short times starts as for the unperturbed process [155], following the law

$$\langle x^2(t) \rangle \approx C_{pH} t^{2Hp}, \tag{49}$$

while at long times the NESS plateau of the MSD emerges, with the height (see Appendix B for the derivation)

$$\langle x^2_{\mathrm{pl}} \rangle \approx C_{pH} \Gamma(2Hp+1)/r^{2Hp}, \tag{50}$$

as shown in Fig. 9. Here C_{pH} is given by Eq. (41) with $D_0 \to D_{0H} = D_0 \bar{K}^2 2K_{2H}$. This general behavior of the MSD is expected and analogous to that of the parent processes of reset FBM and reset HDPs (considered in Secs. III A and IV A, correspondingly).

B. PDF

The approximate PDF of stochastically reset HDP-FBM at intermediate-to-long distances from the origin, given by expression (see Appendix C for the derivation)

$$P(x) \approx \frac{\sqrt{2}r}{\sqrt{2H(2H+1)}} \left(\frac{2Hp^2}{4D_{0H} r} \right)^{\frac{1}{2H+1}} \frac{1}{p} |x|^{\frac{2-p(2H+1)}{p(2H+1)}} \times \exp\left[-\left(\frac{|x|^{2/p} r^{2H}}{D_{0H}(2/p)^2} \right)^{\frac{1}{2H+1}} \left((2H)^{\frac{1}{2H+1}} + (2H)^{-\frac{2H}{2H+1}} \right) \right], \tag{51}$$

is shown in Fig. 10, revealing a good agreement with the results of our computer simulations. We observe a good agreement between theory and simulations at intermediate-to-large separations x, while for small $|x|$ the spike or peak due to resetting emerges (when the conditions of PDF trimodality are satisfied, as described below).

Trimodal PDFs for reset HDP-FBM processes in the NESS are selected as those shapes having three—rather that one or two—points with zero derivative of the PDF with respect to the coordinate. The necessary condition for this is $\gamma < 0$ (subdiffusive parental HDPs) and superdiffusive Hurst exponents H (as we conclude from the region in the plane of $\{H, \gamma\}$ amenable for computer simulations; see Fig. 1 in Ref. [155]). The diagram of trimodal PDF shapes in the plane $\{H, r\}$ for a fixed value of the diffusivity exponent $\gamma = -2$ is presented in Fig. 11. We find that high resetting rates and strongly superdiffusive parental FBMs promote the emergence of PDF trimodality for reset HDP-FBM. Trimodality is clearly a function of the HDP exponent $\gamma < 0$ too (the results of simulations

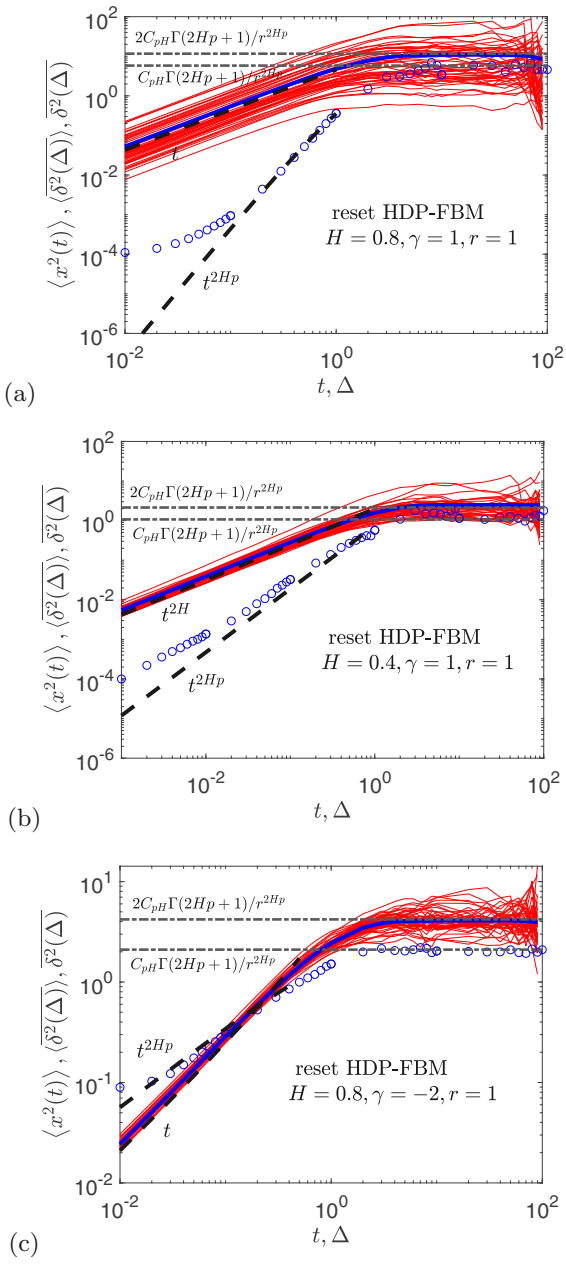

FIG. 9. The same as in Fig. 2 but for the generalized reset HDP-FBM process, computed for the parameters as indicated in the plots. The short-time predictions of Eqs. (50) and (57) and the long-time plateaus of Eqs. (50) and (58) for the MSD and mean TAMSD, respectively, are the dashed and dot-dashed lines.

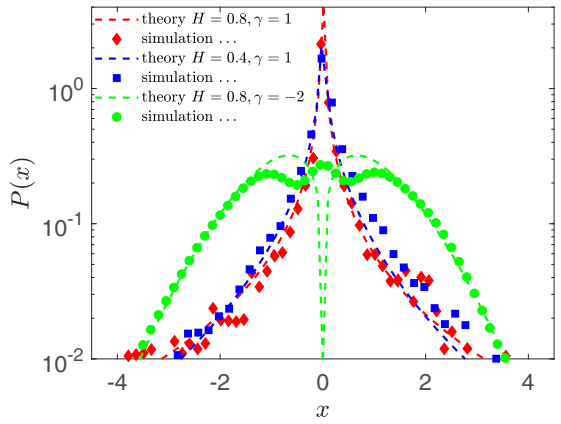

FIG. 10. The same as in Fig. 3 but for reset HDP-FBM plotted for diffusion time $t = T = 10^2$ at the resetting rate $r = 1$ and for the parameters of Fig. 9 (see the legend).

for other γ values are not shown). In the region of large resetting rates r and high Hurst exponents H the PDF peak at the reset position $x = 0$ is most distinctly pronounced.

Note that the domain of HDP exponents $\gamma < 0$ and Hurst exponents $H < 1/2$ is not allowed for our specific simulation procedure employed for HDP-FBM processes [155]: thus, we cannot check if trimodal PDFs are present for HDP-FBM also at $H < 1/2$ and subdiffusive HDPs (the "forbidden region" of parameters). The region of exponent variation in Figs. 25 and 11 is such that only $\gamma < 0$ ($p < 1$) and superdiffusive FBMs with $H > 1/2$ are allowed (again, see Fig. 1 in Ref. [155]).

Now we rationalize the height of the resetting-induced PDF peak at the origin. Because of regularization of subdiffusive HDPs via the diffusivity Ansatz (19), the particles returned to the origin start spreading effectively not according to HDP-FBM, but rather as conventional reset FBM. The PDF peak at $x \approx 0$ cannot be captured by the Laplace-method-based PDF (51) applicable at intermediate-to-large separations from the

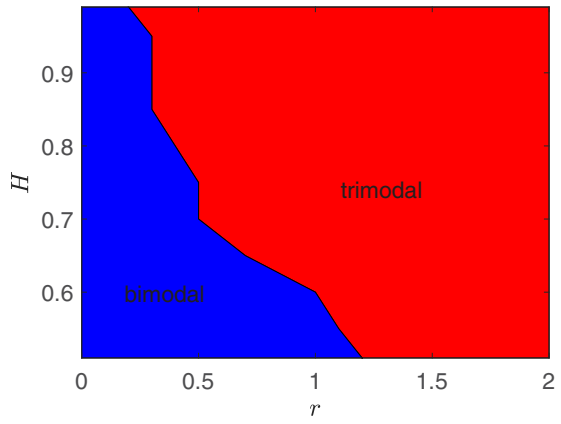

FIG. 11. Diagram of bimodal and trimodal PDF shapes for the reset generalized HDP-FBM process in the plane of resetting rates r and Hurst exponents H, plotted for $\gamma = -2$. The region $0 < H < 1/2$ is not accessible in the simulations of subdiffusive parental HDPs (which are yielding bimodal PDFs being "transferred" into trimodal PDFs by resetting). Other parameters: $T = 10^2$, $dt = 10^{-2}$, $N = 10^4$.

origin. For larger r values, however, the fraction of diffusing particles returned to the origin is comparatively large so that FBM dominates the overall dynamics, while the HDP-based spreading dynamics is not yet established. Therefore, at larger r we expect the scaling for the PDF height at the origin, $P(x = 0)$, for reset HDP-FBM to follow that of simple reset FBM,

$$P(x = 0) \sim r^H, \tag{52}$$

given by Eq. (29). This asymptote is indeed found to fit the results of computer simulations rather closely for the regime of frequent resetting, as illustrated in Fig. 25.

For small r values the PDF value at $x = 0$ is rather HDP-dynamics dominated, as for a free process of HDP-FBM [155]. Therefore, for rare resetting of HDP-FBM we predict the following relation:

$$P(x = 0) \sim r^{pH}. \tag{53}$$

This scaling is reminiscent of that found for free HDP-FBM [155], with the inverse rate of resetting playing the role of the trajectory length T, as intuitively expected,

$$T \leftrightarrow 1/r. \tag{54}$$

Performing simulations for two different simulation time-steps, in Fig. 25 we show that the differences for the heights of the PDF at the origin do exist, but they are not substantial so that the theoretically predicted asymptotic laws (52) and (53) for $P(x = 0)$ are still valid.

C. TAMSD

For reset HDP-FBM for the choice of exponents $0 < H < 1/2$ the leading TAMSD term scales sublinearly as

$$\langle\overline{\delta^2(\Delta)}\rangle \approx C_{pH} r^{-2Hp} \times (r\Delta)^{2H}, \tag{55}$$

while for $1/2 < H < 1$ the leading term grows linearly,

$$\langle\overline{\delta^2(\Delta)}\rangle \approx (1/2)\langle\overline{\delta^2_{\rm pl}}\rangle \times (r\Delta)^1. \tag{56}$$

Generally, the mean TAMSD of the reset HDP-FBM process is a combination of these two terms,

$$\langle\overline{\delta^2(\Delta)}\rangle \approx (1/2)\langle\overline{\delta^2_{\rm pl}}\rangle \times (r\Delta)^1 + C_{pH} r^{-2Hp} \times (r\Delta)^{2H}, \tag{57}$$

whereas at long lag times the mean-TAMSD plateau is realized with twice the height of the MSD plateau given by (50), i.e.,

$$\langle\overline{\delta^2_{\rm pl}}\rangle \approx 2\langle x^2_{\rm pl}\rangle \approx 2 \times C_{pH}\Gamma(2Hp + 1)/r^{2Hp}. \tag{58}$$

These expressions present a natural continuation of the results for reset FBM and HDPs and they enable excellent quantitative fit of the simulation data for varying model parameters and scaling exponents (γ and H), see Fig. 9. We emphasize that the sublinear (55) and linear (56) short-lag-time scaling of the TAMSD for reset HDP-FBM are "inherited" from the respective scaling laws for reset FBM, Eqs. (30) and (31), while the the height of the TAMSD plateau in the NESS given by Eq. (58) depends on the "intensity" of the HDP-driven dynamics, C_{pH}.

Note that for HDPs we generally use slightly nonzero reset positions. In Fig. 9 for $\gamma > 0$ we set

$$x_0 = x_{\rm res} = 10^{-2}, \tag{59}$$

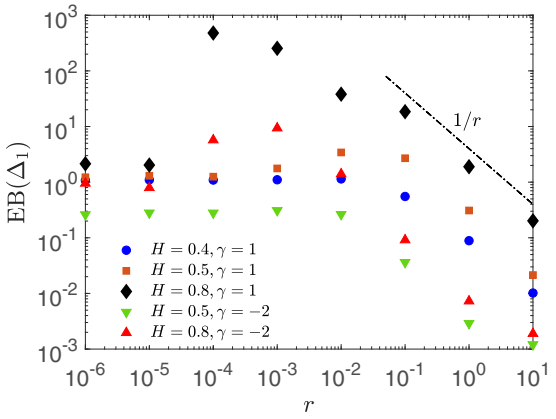

FIG. 12. The same as in Fig. 5, but showing the ergodicity-breaking parameter for the reset HDP-FBM processes EB($\Delta_1 = 10^{-2}$) versus the rate of resetting, for H and γ exponents as indicated in the legend. The asymptote (35) is the black dot-dashed line shown at intermediate-to-large r. Parameters: $T = 10^2$ and $dt = 10^{-2}$.

while for $\gamma < 0$ the reset position was fixed at $x_0 = 0.3$ [to shorten the transient short-time regime where the theoretical and simulation-based MSD results somewhat differ (due to expected effects of initial-position relaxation [151,152])].

D. EB

The spread of individual TAMSDs of stochastically reset HDP-FBM depends—in addition to the leading dependence on resetting rate r—on the values of the Hurst exponent H and the HDP-diffusivity exponent γ. Performing simulations for systematically varying r we observe that, especially for superdiffusive FBM being the parent process for HDP-FBM, the dependence of EB on r is nonmonotonic. Similarly to the EB(r) dependence for reset FBM, the EB(r) for HDP-FBM exhibits a maximum at intermediate rates of resetting. For these conditions, as $r \to 0$ the EB parameter smoothly goes to the respective values for the nonreset process.

In contrast to FBM, for HDP-FBM processes in the absence of resetting the EB values are not small because the parent HDP process is by itself nonergodic, with MSD $\neq$TAMSD and finite EB values even for infinitely long trajectories [151,152] (the general features of EB(p) variation for HDPs are similar to those of CTRWs [152]). Therefore, for the trajectories of a finite length and at $\Delta/T \ll 1$ the variations in the magnitudes of short-lag-time TAMSD realizations—characterizing different TAMSD-based transport coefficients—are distinctly visible.

In the opposite limit of very frequent resetting, again similar to the EB parameter of reset FBM, a power-law decay EB(r, Δ_1) $\sim 1/r$ is detected in simulations, see Fig. 12. This decay of EB(Δ_1) at high rates of reset is universal, being detected for all choices of exponents H and γ of reset HDP-FBM processes, as well as for trajectories of different lengths, see Fig. 26. The detailed analysis of positioning of this EB(r)-maximum as a function of exponents H and γ as well as of trajectory length T is beyond the scope of the current study.

The analysis of whether—for a fixed FBM exponent H and resetting rate r—the spread of TAMSDs increases as the exponent γ deviates from the "most ergodic" value $\gamma = 0$ (expected to yield smallest EB values) toward negative γ for subdiffusive and positive γ for superdiffusive HDPs can also be performed. Its results can then be compared to the theoretical predictions for the EB(γ)-dependence for nonreset HDPs [151]. All these issues deserve a special theoretical consideration (especially if they become relevant for real resetting experiments).

VI. DISCUSSION AND CONCLUSIONS

The current study is a "Pitot drop" [224] to a "tsunami" of recent resetting-related publications. This small contribution contains, however, vital single-trajectory-based concepts of the TAMSD and the distribution of TAMSDs ubiquitously used in the analysis of time series from numerous single-particle-tracking experiments. These concepts will hopefully be useful and productive for theoretical studies of other reset stochastic processes (see Sec. VI C) as well as for experimental resetting setups.

A. Summary of the main results

The constant-rate Poissonian-resetting setup was employed to the initially ergodic long-time-memory process of FBM and the initially nonergodic but Markovian HDPs to study certain resetting effects onto the ensemble- and time-averaged characteristics of the particle-spreading dynamics (in terms of the MSD and TAMSD, the PDF, and the EB). These two widely used processes that are very different in their stochastic nature, as well as the "compound process," exemplify how resetting events can smear out the initial distinctions between FBM and HDPs yielding often similar behaviors for many standard quantifiers, as summarized in Table I.

1. Reset FBM

We detected nonequivalence of the MSD and mean TAMSD for reset superdiffusive and the equivalence for subdiffusive reset FBM. Specifically, we found that both for sub- and superdiffusive FBM the MSD starts (as for free FBM) with $\sim t^{2H}$ scaling, while the TAMSD starts sublinearly in lag time for subdiffusive and linearly for superdiffusive reset FBM. In the long-time limit, both the MSD and mean TAMSD revealed the plateau-like behaviors, with the height of the TAMSD being twice that of the MSD, $\langle \overline{\delta^2_{\rm pl}} \rangle \approx 2\langle x^2_{\rm pl} \rangle$; see also Table I.

Regarding the PDF of reset FBM in the NESS, we quantified in simulations and described analytically the shapes both at intermediate-to-large separations from the origin, as well as the height of the PDF at the origin (representative of the relative fraction of particles returned at the initial position by the restart events).

Depending on the resetting rate r, more frequent resetting was shown to be capable of both impeding and enhancing the degree of spreading of the magnitudes of individual TAMSDs of reset FBM. The nonmonotonic behavior of EB versus r and resetting-induced nonergodicity we discovered in simulations was most pronounced for highly superdiffusive reset FBM, at $H \to 1$. In the strong-resetting limit, we found a sim-

ple power-law decrease $\mathrm{EB}(r) \sim 1/r$ for reset superdiffusive FBM that can be checked/probed experimentally.

2. Reset HDPs

For reset HDPs, at short times we observed the MSD growing unperturbed as $\sim t^p$ and the mean TAMSD growing linearly with the lag time, the same scaling relations as for nonreset HDPs [151,152,155], and thus weak ergodicity-breaking and MSD-TAMSD nonequivalence is observed for reset HDPs (see also Table I). Similarly to reset FBM, for reset HDPs we found that the long-time plateau of the mean TAMSD in the NESS is twice the MSD plateau, as we quantified analytically in excellent agreement with the *in silico* findings. The relation $\langle \overline{\delta^2_{\mathrm{pl}}} \rangle \approx 2\langle x^2_{\mathrm{pl}} \rangle$ valid for all the reset processes studied here is our first key result.

3. Reset HDP-FBM

For the generalized process of reset HDP-FBM we found that upon Poissonian resetting the MSD at short times always starts as $\sim t^{2Hp}$, while the mean TAMSD starts linearly for the super- and sublinearly $\sim \Delta^{2H}$ for the superdiffusive FBM component of reset HDP-FBM. These asymptotes as well as the long-time plateaus with $\langle \overline{\delta^2_{\mathrm{pl}}} \rangle \approx 2\langle x^2_{\mathrm{pl}} \rangle$ observed in computer simulations agree excellently with the theoretical predictions. Apart from reset subdiffusive FBM that remained ergodic upon resetting, other pure and "combined" reset processes we considered here have revealed the nonequivalence of the MSD and mean TAMSD at short (lag) times, see Table I. This omnipresent MSD-TAMSD nonequivalence at short times upon resetting (even for initially ergodic processes) is our second key result.

The shape of the PDF computed analytically with the Laplace method was demonstrated to agree well with the numerical results of our Langevin-equation-based stochastic simulations. For subdiffusive HDPs and superdiffusive FBM contributing to the compound (subdiffusive HDP)-(superdiffusive FBM) reset process we detected a novel class of trimodal shapes of the PDF. We unveiled the domain of existence of these trimodal PDFs, with the general conclusion that more frequent resetting and more superdiffusive Hurst exponents of FBM favor trimodal PDF profiles of reset HDP-FBM. We quantified the scaling relations for the peak of the PDF at the origin (the fraction of particles remaining at the reset position), both theoretically and via simulations.

Note that although trimodal PDF profiles were considered for specific setups of noninstantaneous resetting for the normal dynamics with certain position-dependent functional forms of the reset speed [45], the trimodal PDFs we unveiled for reset (subdiffusive HDP)-(superdiffusive FBM) processes are new and universal, being based on the underlying dynamics of the "source" processes of subdiffusive HDPs with a bimodal PDF and superdiffusive FBM. This emerging PDF trimodality in the NESS for reset subdiffusive HDPs and respective HDP-FBM is our third key result. Such trimodal PDFs can be realizable in diffusion-resetting protocols, even with instant returning of particles to the restart position.

For the EB parameter, similarly to that of reset FBM, at high rates of resetting we discovered a universal power-law decrease $\mathrm{EB}(r) \sim 1/r$, with the exact values of EB being sensitive to the values of dynamics-governing exponents H and γ. At small resetting rates the EB values approach those of the nonreset process, as expected, while a pronounced maximum of $\mathrm{EB}(r)$ and, thus, resetting-induced nonergodicity emerges at intermediate r. This universal nonmonotonic $\mathrm{EB}(r)$-dependence—with a prominent maximum followed by $\mathrm{EB}(r) \propto 1/r$-decay at large r—is our fourth key result.

We conclude here stating that the behaviors of the MSD and mean TAMSD in the NESS for FBM, HDPs, and HDP-FBM processes under exponential resetting are functionally *remarkably similar*, alike the found effect of the nonmonotonic variation of EB versus resetting rate. High-rate exponential resetting (naturally) *smears out* the distinctions between initially very different processes we studied here, yielding in the long-time limit similar—possibly, also for other processes under such resetting—functional dependencies for the TAMSD and EB.

B. Possible effects of initial conditions

We employed the standard [and experimentally relevant] concept of ergodicity as the equivalence of the MSD and mean TAMSD at short times and quantified the spread of individual TAMSDs at $\Delta = \Delta_1 = dt$ in terms of EB. The initial particle positions were always kept fixed. These conditions are realizable experimentally, with the MSD being computed without subtracting this [nearly zero] initial position, x_0. From the theoretical perspective, however, considering initial positions of particles being *distributed* according to the long-time PDF in the NESS, $P(x_0)$, creates another statistical ensemble and, thus, offers a different approach to compute averages. The ensemble- and x_0-averaged MSD after this additional averaging, $\langle\langle (x(t) - x_0)^2 \rangle_{P(x_0)}\rangle$, can be a more *theoretically rigorous* measure for assessing the degree of nonergodicity and MSD-TAMSD nonequivalence.

We refer the reader to the study [221] regarding the impact of the starting positions being fixed versus being distributed with the equilibrium PDF on the properties of diffusion in a parabolic potential, the Ornstein-Uhlenbeck process. It was found, *inter alia*, that the MSD-TAMSD nonequivalence at short lag times indeed *disappears* when the MSD involves second averaging over $P_{\mathrm{eq}}(x_0)$ of all possible starting positions being sampled from the equilibrium-state PDF, $\langle\langle (x(t) - x_0)^2 \rangle_{P_{\mathrm{eq}}(x_0)}\rangle$. The "confining" Ornstein-Uhlenbeck process is similar to resetting-based protocols also in terms of long-time MSD/TAMSD plateaus featuring $\langle \overline{\delta^2_{\mathrm{pl}}} \rangle / \langle x^2_{\mathrm{pl}} \rangle = 2$ [again, for the starting positions distributed with $P_{\mathrm{eq}}(x_0)$] [221]. The effects of distributed x_0-positions onto nonergodicity of various reset anomalous-diffusion processes will be the subject of our future investigations.

C. Applications and further developments

Our TAMSD-based approach to reset stochastic processes seems more natural for examining the continuous trajectories, emerging, e.g., as outputs in single-particle-tracking experiments, as compared to the MSD-based methods. Some methods for the analysis of abrupt transitions and the detection of change-points in time series, *inter alia*, in the presence

of measurement uncertainties, were developed recently [225] and applied to predicting the moments of several economic crashes. With our quantifiers, the predicted differences in the short-lag-time scaling of the mean TAMSD for reset FBM—namely, a sublinear and linear TAMSD growth depending on the value of Hurst exponents, see Sec. III C—could help us to assess (e.g., upon varying H and comparing with the MSD growth) if the underlying dynamics is indeed of FBM-type.

Straightforward future developments of this study is to apply the TAMSD- and EB-based formulation to other stochastic processes with a resetting dynamics imposed—such as CTRWs [16,37,38,55,62,71,130,226], Lévy walks/flights [227], SBM [53,54,131], exponential SBM [137], diffusion with multiple mobility states, the Ornstein-Uhlenbeck process [221,222], geometric BM [228–232], diffusion models with distributed [233,234], and "diffusing diffusivity" [150,235–243] as well as various "hybrid" processes (SBM-HDPs [132], FBM-(diffusing diffusivity) [21], SBM-(diffusing diffusivity) [135], etc.). Also, one can employ other types of resetting protocols [periodic, power-law, and other functional forms for $\psi(r)$ distributions; resetting when particular $x_{\max}$ values are reached, to distributed resetting points, with memory effects, etc.] and to consider the underdamped versions [135,137] of anomalous-diffusion processes (with the initially ballistic MSD) with resetting to unveil the differences from the behaviors reported here for reset FBM, HDPs, and HDP-FBM as well as to mimic relevant experimental situations.

Recently, an experimental realization of diffusion of a colloidal particle with resetting implemented via holographic optical tweezers was reported [67], possibly allowing position- or energy-dependent resetting of trap-confined beads [36] and dragging particles [73] in external traps. The ability and sensitivity of such optical-trap-based setups to infer the underlying stochastic process governing the particles' motion—as a function of resetting conditions and other relevant parameters—remains to be quantified. Moreover, performing such optical-traps experiments with micron-sized beads in crowded environments of living cells—to infer whether FBM or viscoelastic diffusion or restricted/compartmentalized diffusion is at play—can potentially have additional complications.

We hope that the theoretical and experimental resetting communities will find the current time-averaging single-trajectory-based approach—with the concepts of TAMSDs and TAMSD-irreproducibility embodied by the EB parameter—useful to infer the degree of nonergodicity for other diffusion models and real physical systems in the presence of [stochastic] resetting dynamics.

ACKNOWLEDGMENTS

A.G.C. gratefully acknowledges the Humboldt University of Berlin for hospitality and support. R.M. acknowledges financial support by the Deutsche Forschungsgemeinschaft (DFG Grants No. ME 1535/7-1 and No. ME 1535/12-1). R.M. thanks the Foundation for Polish Science (Fundacja na rzecz Nauki Polskiej) for support within an Alexander von Humboldt Polish Honorary Research Scholarship.

APPENDIX A: TAMSD OF RESET FBM: SHORT LAG TIMES

We start with the autocorrelation function of FBM with Poissonian resetting at a rate r obtained in Ref. [42],

$$\langle x(t+\Delta)x(t)\rangle = K_{2H}e^{-r\Delta}\left\{\int_0^t re^{-r\tau}\left(\tau^{2H}+(\tau+\Delta)^{2H}-\Delta^{2H}\right)d\tau + e^{-rt}(t^{2H}+(t+\Delta)^{2H}-\Delta^{2H})\right\}, \tag{A1}$$

and with the expression for the MSD of SBM under a constant-rate resetting (substituting the SBM exponent α via the Hurst exponent H of FBM as $\alpha = 2H$) [53,54]

$$\langle x^2(t)\rangle = 2K_{2H}t^{2H}e^{-rt} + 2K_{2H}r^{-2H}\gamma(2H+1, rt), \tag{A2}$$

where the (lower) incomplete Gamma function is

$$\gamma(a,z) = \int_0^z e^{-x}x^{a-1}dx. \tag{A3}$$

The TAMSD of Eq. (9), with the integrand

$$\langle[x(t+\Delta)-x(t)]^2\rangle = \langle x^2(t+\Delta)\rangle + \langle x^2(t)\rangle - 2\langle x(t+\Delta)x(t)\rangle, \tag{A4}$$

can then be presented as a combination of two terms

$$\begin{aligned}\langle\overline{\delta^2(\Delta)}\rangle = {}& \frac{2K_{2H}}{T-\Delta}\int_0^{T-\Delta}dt\{(t+\Delta)^{2H}e^{-r(t+\Delta)} \\ & + t^{2H}e^{-rt} - e^{-r\Delta}e^{-rt}(t^{2H}+(t+\Delta)^{2H}-\Delta^{2H})\} \\ & + \frac{2K_{2H}}{T-\Delta}\int_0^{T-\Delta}dt\Big\{r^{-2H}\gamma(2H+1, r(t+\Delta)) \\ & + r^{-2H}\gamma(2H+1, rt) \\ & - e^{-r\Delta}\int_0^t re^{-r\tau}(\tau^{2H}+(\tau+\Delta)^{2H}-\Delta^{2H})d\tau\Big\}.\end{aligned} \tag{A5}$$

In the limit of vanishing lag times, at $\Delta/T \ll 1$, at the condition of multiple resetting events within a trajectory of length T, given by

$$rT \gg 1, \tag{A6}$$

the first integral in Eq. (A5) can be neglected compared to the second term. The second term (after taking the integrals) yields the approximate result for the TAMSD

$$\begin{aligned}\langle\overline{\delta^2(\Delta)}\rangle \approx {}& \frac{2K_{2H}}{T-\Delta}\int_0^{T-\Delta}dt\left\{(1-e^{-r\Delta})r^{-2H}\gamma(2H+1, rt)\right. \\ & \left. + \Delta^{2H}e^{-r\Delta}(1-e^{-rt})\right\}.\end{aligned} \tag{A7}$$

In the limit of long enough trajectories and short enough lag times, at

$$r\Delta \ll 1, \tag{A8}$$

the first term in the integrand of Eq. (A7) yields that for

$$2 > 2H > 1 \tag{A9}$$

the leading TAMSD behavior is given by

$$\langle\overline{\delta^2(\Delta)}\rangle \approx 2K_{2H}\Gamma(2H+1)r^{1-2H} \times \Delta^1. \tag{A10}$$

On the contrary, for

$$0 < 2H < 1, \tag{A11}$$

the second term in Eq. (A7) gives the leading contribution to the short-lag-time TAMSD asymptotic that is sublinear in Δ,

$$\langle\overline{\delta^2(\Delta)}\rangle \approx 2K_{2H} \times \Delta^{2H}. \tag{A12}$$

The asymptotes of Eqs. (A10) and (A12)—which are the asymptotic relations (30) and (31) in the main text—can clearly be obtained also via first expanding the integrand of the TAMSD in Eq. (A5) for small Δ and then taking the limit of long times (not shown in detail).

APPENDIX B: MSD OF RESET HDP-FBM

For the resetting dynamics of a stochastic process with the Gaussian PDF for particle displacements $P_0(x,t)$ in the presence of exponential resetting [a constant rate of resetting, Eq. (2)], the PDF of the reset process $P(x,t)$ can be expressed via the PDF of the unperturbed process $P_0(x,t)$ through [53,54]

$$P(x,t) = e^{-rt}P_0(x,t) + \int_0^t re^{-r\tau} \times P_0(x,\tau)d\tau. \tag{B1}$$

The first term in Eq. (B1) signifies the probability of no resetting events taking place from time 0 to time t (with the exponentially decaying probability of such an event), while the second term integrates over all multiple resetting events possible to occur in incremental time-steps during the same time period. Multiplying both sides of Eq. (B1) by x^2 and integrating over all possible particle positions one gets for the MSD of the reset HDP-FBM process that

$$\langle x^2(t)\rangle = e^{-rt}C_{pH}t^{2Hp} + C_{pH}r^{-2Hp} \times \gamma(2Hp+1, rt), \tag{B2}$$

where the definitions and notations (41) and (A3) are used. The height of the MSD plateau at long times [for $rt \gg 1$ and many resetting events taking place by time t (long-time limit of the NESS)] is dominated by the second term in Eq. (B2),

$$\langle x_{\rm pl}^2\rangle \approx C_{pH}\Gamma(2Hp+1)/r^{2Hp}, \tag{B3}$$

that yields Eq. (50) in the main text. At short times (when the condition $rt \ll 1$ is satisfied) the Taylor expansion of Eq. (B2) yields that the MSD starts nearly unperturbed, as [155]

$$\langle x^2(t)\rangle \approx C_{pH}t^{2Hp}, \tag{B4}$$

that gives Eqs. (39) and (49) in the main text.

APPENDIX C: PDF OF RESET HDP-FBM

Starting with the PDF of HDP-FBM in the absence of resetting [155],

$$P(x,t) = \frac{|x|^{1/p-1}}{\sqrt{4\pi D_{0H}t^{2H}}}\exp\left[-\left(\frac{|x|^{1/p}}{(2/p)\sqrt{D_{0H}t^{2H}}}\right)^2\right], \tag{C1}$$

and using the relation (B1) connecting the nonreset and the reset PDFs, in the limit of long times (when the term of no-resetting up to time t, $e^{-rt}P_0(x,t)$ in Eq. (B1), can be neglected) we arrive at

$$P(x,t) \approx r\frac{|x|^{1/p-1}}{\sqrt{4\pi D_{0H}}}\int_0^t e^{-r\tau}\tau^{-H}e^{-D_{pH}(x)\tau^{-2H}}d\tau, \tag{C2}$$

where we defined for brevity

$$D_{pH}(x) = |x|^{2/p}/[D_{0H}(2/p)^2]. \tag{C3}$$

Following the strategy outlined in Ref. [53,54] for the PDF of reset SBM, we use the Laplace method to approximate the exponent-containing integral in Eq. (C2). The maximum of a negative-power exponent in Eq. (C2) is achieved at the minimum of its argument, namely, at

$$\tau_{\rm min} = [2HD_{pH}(x)/r]^{\frac{1}{2H+1}}. \tag{C4}$$

This yields for the second derivative

$$(r\tau + D_{pH}(x)\tau^{-2H})''_{\tau,\tau}|_{\tau_{\rm min}} = 2H(2H+1)D_{pH}(x) \times \tau_{\rm min}^{-2H-2}, \tag{C5}$$

so that the power of the exponent becomes

$$r\tau_{\rm min} + D_{pH}(x)\tau_{\rm min}^{-2H} = r^{\frac{2H}{2H+1}}[D_{pH}(x)]^{\frac{1}{2H+1}}\left((2H)^{\frac{1}{2H+1}} + (2H)^{-\frac{2H}{2H+1}}\right). \tag{C6}$$

For the prefactor of the exponent in the resulting PDF, $\exp[-(r\tau_{\rm min} + D_{pH}\tau_{\rm min}^{-2H})]$, obtained after applying the Laplace method to Eq. (C2), one gets

$$r\frac{|x|^{1/p-1}}{\sqrt{4\pi D_{0H}}}\sqrt{\frac{2\pi}{2H(2H+1)D_{pH}(x)\tau_{\rm min}^{-2H-2}}}\tau_{\rm min}^{-H} = \frac{\sqrt{2}r}{\sqrt{2H(2H+1)}}\left(\frac{2Hp^2}{4D_{0H}r}\right)^{\frac{1}{2H+1}}\left(\frac{1}{p}\right)|x|^{\frac{2-p-2Hp}{p+2Hp}}. \tag{C7}$$

Combining (C6) with (C7) and substituting the explicit x-dependence of D_{pH} from Eq. (C3), we arrive at the final approximate result for the PDF of HDP-FBM in Eq. (51) of the main text,

$$P(x) \approx \frac{\sqrt{2}r}{\sqrt{2H(2H+1)}}\left(\frac{2Hp^2}{4D_{0H}r}\right)^{\frac{1}{2H+1}}\frac{1}{p}|x|^{\frac{2-p(2H+1)}{p(2H+1)}} \times \exp\left[-\left(\frac{|x|^{2/p}r^{2H}}{D_{0H}(2/p)^2}\right)^{\frac{1}{2H+1}}\left((2H)^{\frac{1}{2H+1}} + (2H)^{-\frac{2H}{2H+1}}\right)\right]. \tag{C8}$$

Naturally, in the absence of space-dependent diffusion (when the MSD is linear, $p = 1$) the NESS PDF of HDP-FBM Eq. (51) turns after putting $2H = \alpha$ into the PDF of SBM with fully renewal resetting [53,54]; see also Eq. (26).

APPENDIX D: SUPPLEMENTARY FIGURES

Here we present some auxiliary figures supporting the claims in the main text, see Figs. 13–26.

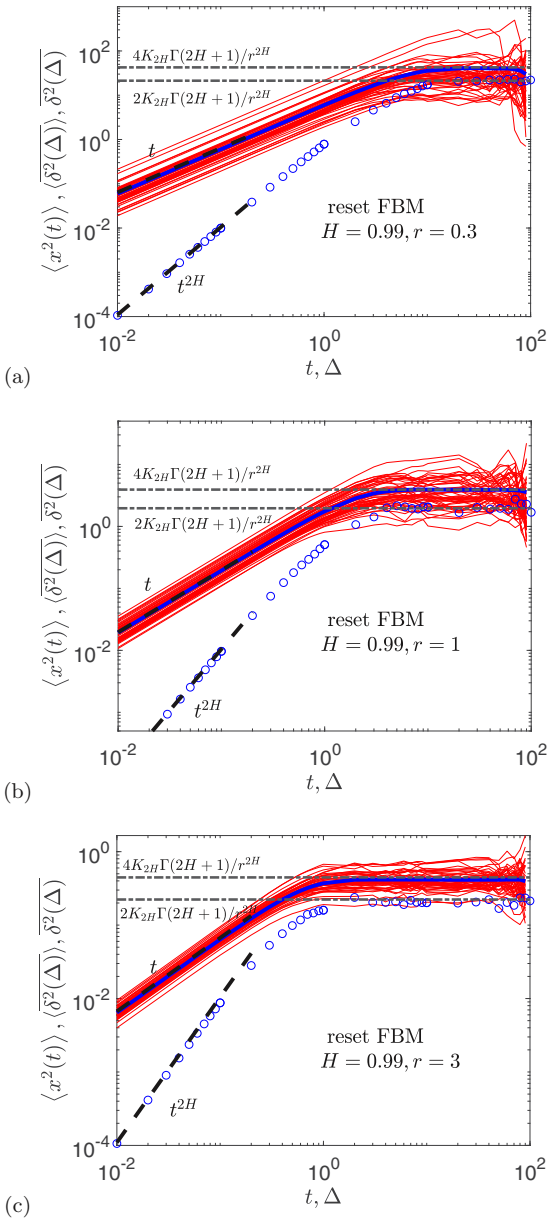

FIG. 13. The same as in Fig. 2, for the same parameters, except for $H = 0.99$ and varying resetting rate r (the values are indicated in the plots), with the same asymptotes shown.

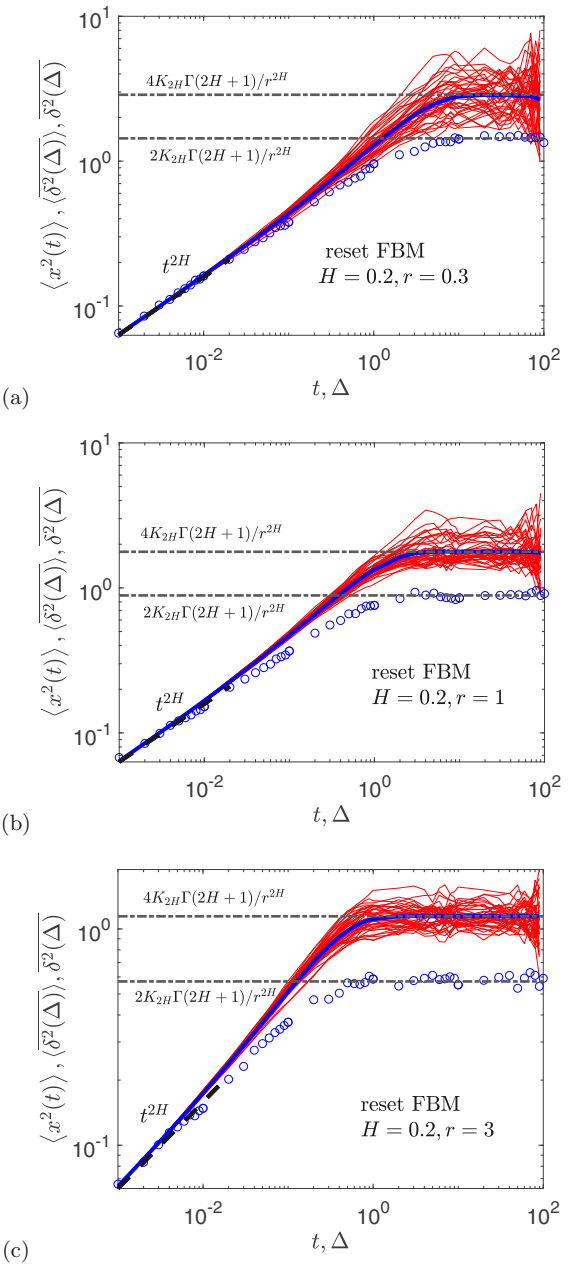

FIG. 14. The same as in Fig. 13, for the same parameters except for $H = 0.2$ and $dt = 10^{-3}$, computed for varying rate of resetting r.

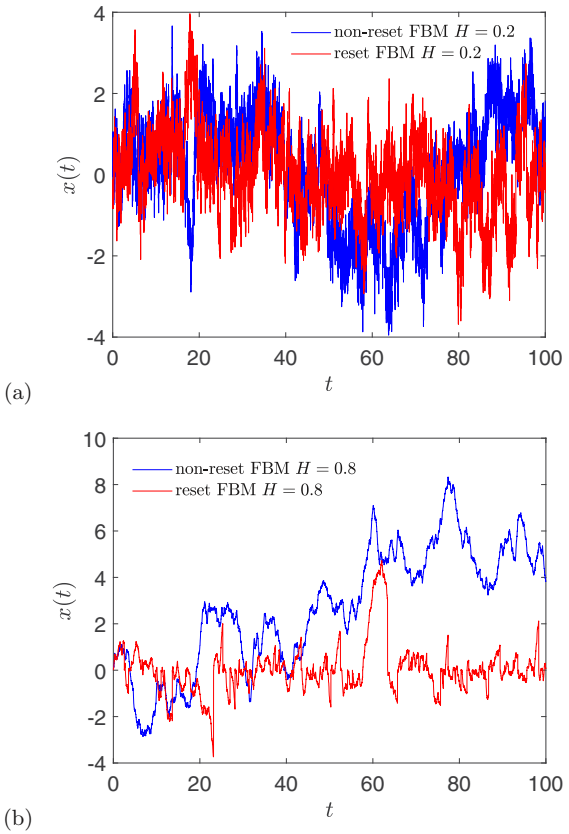

FIG. 15. Exemplary trajectories of reset (red) and nonreset (blue) FBM for $H = 0.2$ for panel (a) and $H = 0.8$ for panel (b), with other parameters being the same as in Fig. 2.

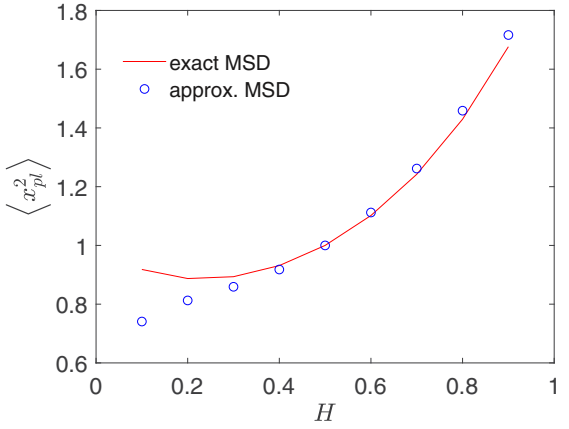

FIG. 16. Comparison of the MSD plateaus of reset FBM in the NESS between Eq. (25) and using the approximate PDF form of Eq. (26), plotted for varying Hurst exponents.

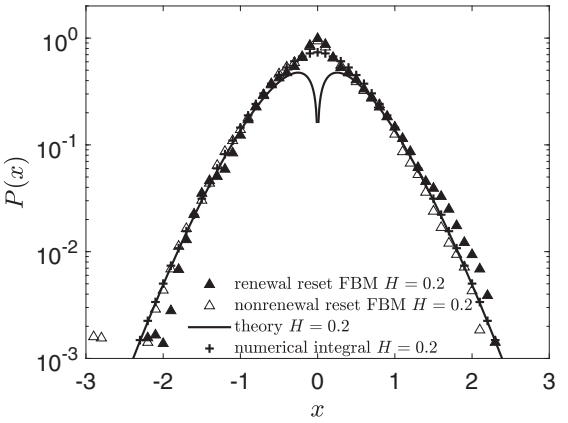

FIG. 17. The same as in Fig. 3, for $r = 10$, $dt = 10^{-2}$, and $H = 0.2$. The results of numerical integration of the exact PDF expression Eq. (B1) are the cross symbols.

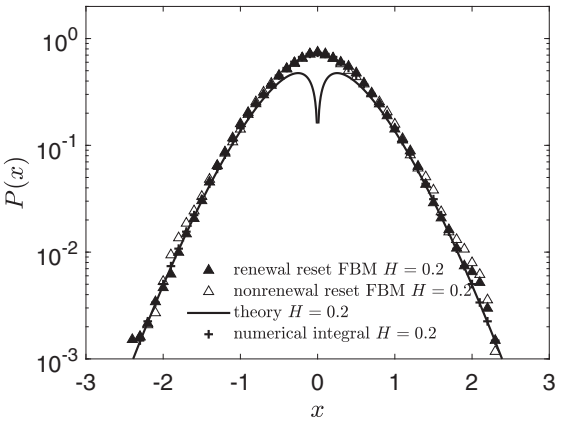

FIG. 18. The same as in Fig. 17, for the same parameters, except for $dt = 10^{-3}$ and $r = 10$ being used in simulations.

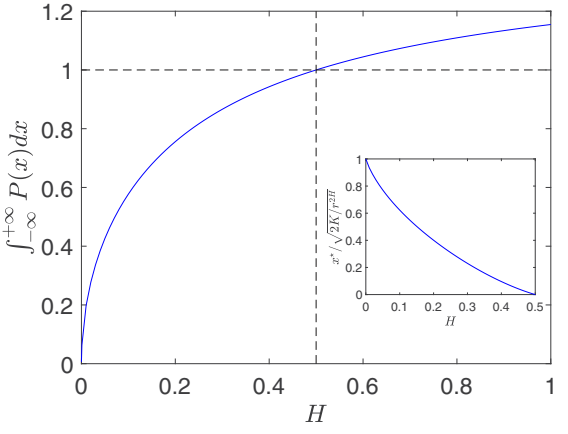

FIG. 19. Variation of the integral of the approximate Laplace-method PDF given by Eq. (26), computed numerically versus the Hurst exponent H. The inset shows the normalized separation $x^\star$ expressed by Eq. (28) versus H.

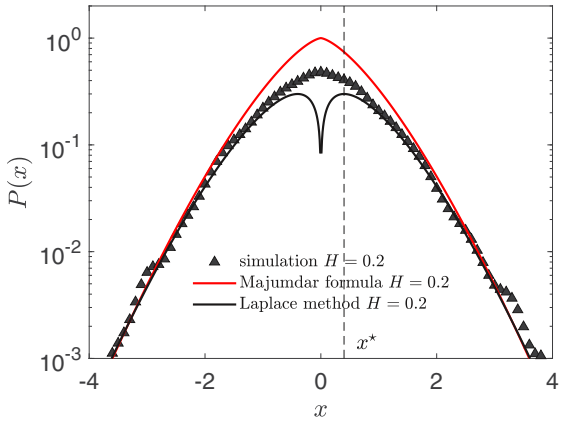

FIG. 20. Results of simulations of subdiffusive reset FBM compared to the PDF (26) and to the leading decay law (27) (derived first in Appendix 1 of Ref. [25]). The threshold separation (28) is the dotted line. Parameters: $T = 10^2$, $dt = 10^{-2}$, $H = 0.2$, and $r = 1$.

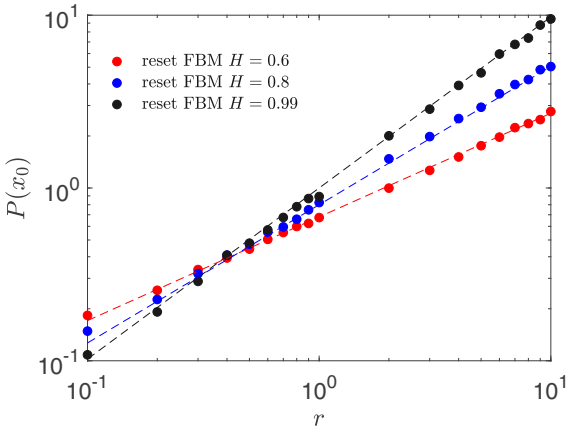

FIG. 21. PDF values of reset FBM at $x = 0$ shown for varying reset rates and for different Hurst exponents. The theoretical predictions (29) are the dashed lines of the respective color. Parameters: $T = 10^2$ and $dt = 10^{-2}$.

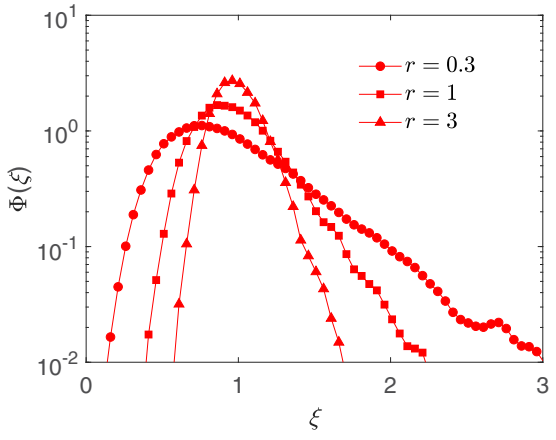

FIG. 22. Scatter distribution of TAMSD amplitudes, defined as $\phi[\xi(\Delta)]$ in Eq. (12), computed at the shortest lag time $\Delta = \Delta_1 = 10^{-2}$ for reset superdiffusive FBM with $H = 0.8$ and for $r = 0.3, 1, 3$, with other parameters being the same as in Fig. 2(c).

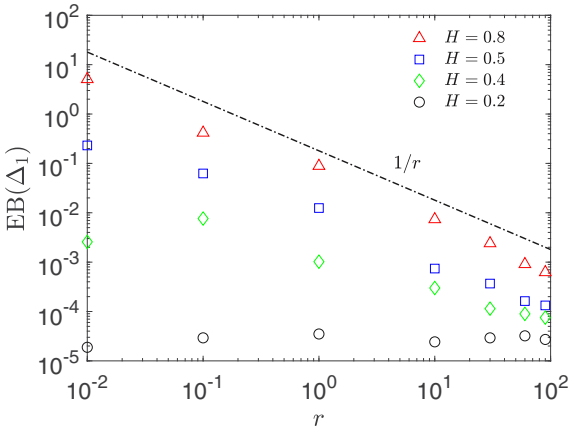

FIG. 23. The same as in Fig. 5, for the same parameters, except for $dt = \Delta_1 = 10^{-3}$.

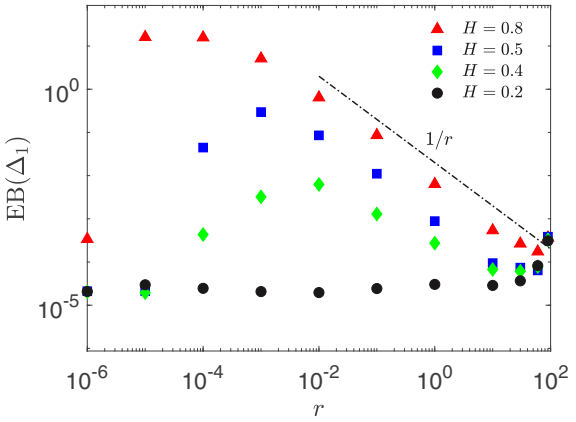

FIG. 24. The same as in Fig. 5, with EB computed at $\Delta_1 = 10^{-2}$, for the same parameters except for $T = 10^3$ (see the legend).

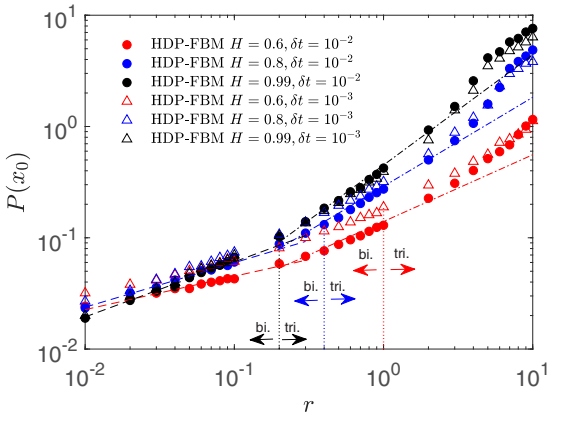

FIG. 25. PDF values of the reset HDP-FBM process for $p = 1/2$ (or $\gamma = -2$), with the regions of bimodal (rare resetting) and trimodal (frequent resetting) PDF shapes being indicated for each choice of the Hurst exponent, computed at $x = x_0 = 0.01$ from computer simulations. The analytical asymptotes (29) and (53) are the dashed lines of the corresponding color shown, respectively, in the regime of large and small rates of resetting. The simulation data for $dt = 10^{-2}$ and 10^{-3} are shown by filled and empty symbols, correspondingly. Parameters: $T = 10$ with $dt = 10^{-3}$ and $T = 10^2$ with $dt = 10^{-2}$, see the legend for details, while ensemble averaging executed over $N = 8000$ HDP-FBM trajectories.

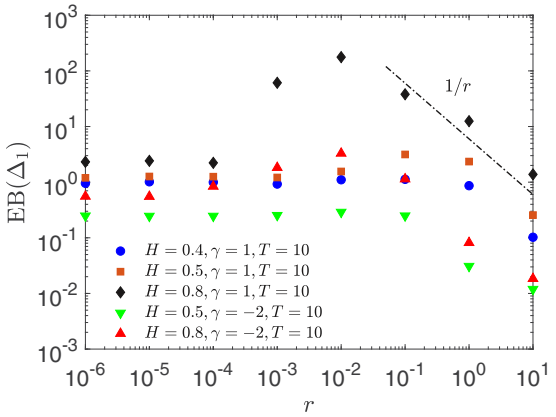

FIG. 26. The same as in Fig. 12, for the same parameters, except for $T = 10$.

APPENDIX E

BM: Brownian motion;
SBM: scaled BM;
FBM: fractional BM;
HDPs: heterogeneous diffusion processes;
CTRWs: continuous-time random walks;
PDF: probability density function;
MSD: mean-squared displacement;
TAMSD: time-averaged MSD;
NESS: nonequilibrium stationary state.

[1] J.-P. Bouchaud and A. Georges, Anomalous diffusion in disordered media: Statistical mechanisms, models and physical applications, Phys. Rep. **195**, 127 (1990).

[2] R. Metzler and J. Klafter, The random walk's guide to anomalous diffusion: A fractional dynamics approach, Phys. Rep. **339**, 1 (2000).

[3] S. Burov, J.-H. Jeon, R. Metzler, and E. Barkai, Single particle tracking in systems showing anomalous diffusion: the role of weak ergodicity breaking, Phys. Chem. Chem. Phys. **13**, 1800 (2011).

[4] I. M. Sokolov, Models of anomalous diffusion in crowded environments, Soft Matter **8**, 9043 (2012).

[5] E. Barkai, Y. Garini, and R. Metzler, Strange kinetics of single molecules in living cells, Phys. Today **65**(8), 29 (2012).

[6] F. Höfling and T. Franosch, Anomalous transport in the crowded world of biological cells, Rep. Prog. Phys. **76**, 046602 (2013).

[7] Y. Meroz, I. M. Sokolov, and J. Klafter, Test for Determining a Subdiffusive Model in Ergodic Systems from Single Trajectories, Phys. Rev. Lett. **110**, 090601 (2013).

[8] R. Metzler, J.-H. Jeon, A. G. Cherstvy, and E. Barkai, Anomalous diffusion models and their properties: Nonstationarity, nonergodicity, and ageing at the centenary of single particle tracking, Phys. Chem. Chem. Phys. **16**, 24128 (2014).

[9] Y. Meroz and I. M. Sokolov, A toolbox for determining subdiffusive mechanisms, Phys. Rep. **573**, 1 (2015).

[10] M. A. F. dos Santos, Analytic approaches of the anomalous diffusion: A review, Chaos, Solitons Fractals **124**, 86 (2019).

[11] S. C. Manrubia and D. H. Zanette, Stochastic multiplicative processes with reset events, Phys. Rev. E **59**, 4945 (1999).

[12] A. Montanari and R. Zecchina, Optimizing Searches Via Rare Events, Phys. Rev. Lett. **88**, 178701 (2002).

[13] M. R. Evans and S. N. Majumdar, Diffusion with Stochastic Resetting, Phys. Rev. Lett. **106**, 160601 (2011).

[14] M. R. Evans and S. N. Majumdar, Diffusion with optimal resetting, J. Phys. A **44**, 435001 (2011).

[15] M. R. Evans, S. N. Majumdar, and K. Mallick, Optimal diffusive search: nonequilibrium resetting versus equilibrium dynamics, J. Phys. A **46**, 185001 (2013).

[16] M. Montero and J. Villarroel, Monotonic continuous-time random walks with drift and stochastic reset events, Phys. Rev. E **87**, 012116 (2013).

[17] S. Gupta, S. N. Majumdar, and G. Schehr, Fluctuating Interfaces Subject to Stochastic Resetting, Phys. Rev. Lett. **112**, 220601 (2014).

[18] M. R. Evans and S. N. Majumdar, Diffusion with resetting in arbitrary spatial dimension, J. Phys. A **47**, 285001 (2014).

[19] L. Kusmierz, S. N. Majumdar, S. Sabhapandit, and G. Schehr, First Order Transition for the Optimal Search Time of Lévy Flights with Resetting, Phys. Rev. Lett. **113**, 220602 (2014).

[20] D. Boyer and C. Solis-Salas, Random Walks with Preferential Relocations to Places Visited in the Past and Their Application to Biology, Phys. Rev. Lett. **112**, 240601 (2014).

[21] X. Durang, M. Henkel, and H. Park, The statistical mechanics of the coagulation-diffusion process with a stochastic reset, J. Phys. A **47**, 045002 (2014).

[22] S. Reuveni, M. Urbakh, and J. Klafter, Role of substrate unbinding in Michaelis-Menten enzymatic reactions, Proc. Natl. Acad. Sci. USA **111**, 4391 (2014).

[23] T. Rotbart, S. Reuveni, and M. Urbakh, Michaelis-Menten reaction scheme as a unified approach toward the optimal restart problem, Phys. Rev. E **92**, 060101(R) (2015).

[24] J. M. Meylahn, S. Sabhapandit, and H. Touchette, Large deviations for Markov processes with resetting, Phys. Rev. E **92**, 062148 (2015).

[25] S. N. Majumdar, S. Sabhapandit, and G. Schehr, Dynamical transition in the temporal relaxation of stochastic processes under resetting, Phys. Rev. E **91**, 052131 (2015).

[26] A. Pal, Diffusion in a potential landscape with stochastic resetting, Phys. Rev. E **91**, 012113 (2015).

[27] S. N. Majumdar, S. Sabhapandit, and G. Schehr, Random walk with random resetting to the maximum position, Phys. Rev. E **92**, 052126 (2015).

[28] C. Christou, and A. Schadschneider, Diffusion with resetting in bounded domains, J. Phys. A **48**, 285003 (2015).

[29] S. Eule and J. J. Metzger, Nonequilibrium steady states of stochastic processes with intermittent resetting, New J. Phys. **18**, 033006 (2016).

[30] S. Reuveni, Optimal Stochastic Restart Renders Fluctuations in First Passage Times Universal, Phys. Rev. Lett. **116**, 170601 (2016)

[31] A. Nagar and S. Gupta, Diffusion with stochastic resetting at power-law times, Phys. Rev. E **93**, 060102(R) (2016).

[32] J. Fuchs, S. Goldt, and U. Seifert, Stochastic thermodynamics of resetting, Europhys. Lett. **113**, 60009 (2016).

[33] E. Roldan, A. Lisica, D. Sanchez-Taltavull, and S. W. Grill, Stochastic resetting in backtrack recovery by RNA polymerases, Phys. Rev. E **93**, 062411 (2016).

[34] A. Pal, A. Kundu, and M. R. Evans, Diffusion under time-dependent resetting, J. Phys. A **49**, 225001 (2016).

[35] A. Pal and S. Reuveni, First Passage Under Restart, Phys. Rev. Lett. **118**, 030603 (2017).

[36] E. Roldan and S. Gupta, Path-integral formalism for stochastic resetting: Exactly solved examples and shortcuts to confinement, Phys. Rev. E **96**, 022130 (2017).

[37] V. P. Shkilev, Continuous-time random walk under time-dependent resetting, Phys. Rev. E **96**, 012126 (2017).

[38] M. Montero, A. Maso-Puigdellosas, and J. Villarroel, Continuous-time random walks with reset events, Eur. Phys. J. B **90**, 176 (2017).

[39] R. Falcao and M. R. Evans, Interacting Brownian motion with resetting, J. Stat. Mech. (2017) 023204.

[40] M. R. Evans and S. N. Majumdar, Run and tumble particle under resetting: A renewal approach, J. Phys. A **51**, 475003 (2018).

[41] A. V. Chechkin and I. M. Sokolov, Random Search with Resetting: A Unified Renewal Approach, Phys. Rev. Lett. **121**, 050601 (2018).

[42] S. N. Majumdar and G. Oshanin, Spectral content of fractional Brownian motion with stochastic reset, J. Phys. A **51**, 435001 (2018).

[43] A. Chatterjee, C. Christou, and A. Schadschneider, Diffusion with resetting inside a circle, Phys. Rev. E **97**, 062106 (2018).

[44] C. Christou, Non-equilibrium stochastic models: random average process and diffusion with resetting, Ph.D. thesis, Universität zu Köln, 2019.

[45] A. Pal, L. Kusmierz, and S. Reuveni, Invariants of motion with stochastic resetting and space-time coupled returns, New J. Phys. **21**, 113024 (2019).

[46] A. Pal and V. V. Prasad, Landau-like expansion for phase transitions in stochastic resetting, Phys. Rev. Res. **1**, 032001(R) (2019).

[47] A. Pal, L. Kusmierz, and S. Reuveni, Time-dependent density of diffusion with stochastic resetting is invariant to return speed, Phys. Rev. E **100**, 040101(R) (2019).

[48] D. Gupta, Stochastic resetting in underdamped Brownian motion, J. Stat. Mech. (2019) 033212.

[49] M. A. F. dos Santos, Fractional Prabhakar derivative in diffusion equation with non-static stochastic resetting, MDPI: Physics **1**, 40 (2019).

[50] A. Maso-Puigdellosas, D. Campos, and V. Mendez, Transport properties and first-arrival statistics of random motion with stochastic reset times, Phys. Rev. E **99**, 012141 (2019).

[51] J. Masoliver, Telegraphic processes with stochastic resetting, Phys. Rev. E **99**, 012121 (2019).

[52] T. Robin, L. Hadany, and M. Urbakh, Random search with resetting as a strategy for optimal pollination, Phys. Rev. E **99**, 052119 (2019).

[53] A. S. Bodrova, A. V. Chechkin, and I. M. Sokolov, Nonrenewal resetting of scaled Brownian motion, Phys. Rev. E **100**, 012119 (2019).

[54] A. S. Bodrova, A. V. Chechkin, and I. M. Sokolov, Scaled Brownian motion with renewal resetting, Phys. Rev. E **100**, 012120 (2019).

[55] A. S. Bodrova and I. M. Sokolov, Continuous-time random walks under power-law resetting, Phys. Rev. E **101**, 062117 (2020).

[56] A. S. Bodrova and I. M. Sokolov, Brownian motion under noninstantaneous resetting in higher dimensions, Phys. Rev. E **102**, 032129 (2020).

[57] A. S. Bodrova and I. M. Sokolov, Resetting processes with noninstantaneous return, Phys. Rev. E **101**, 052130 (2020).

[58] G. Mercado-Vasquez, D. Boyer, S. N. Majumdar, and G. Schehr, Intermittent resetting potentials, J. Stat. Mech. (2020) 113203.

[59] M. R. Evans, S. N. Majumdar, and G. Schehr, Stochastic resetting and applications, J. Phys. A **53**, 193001 (2020).

[60] C. A. Plata, D. Gupta, and S. Azaele, Asymmetric stochastic resetting: Modeling catastrophic events, Phys. Rev. E **102**, 052116 (2020).

[61] S. Ray, Space-dependent diffusion with stochastic resetting: A first-passage study, J. Chem. Phys. **153**, 234904 (2020).

[62] T. Zhou, P. Xu, and W. Deng, Continuous-time random walks and Lévy walks with stochastic resetting, Phys. Rev. Res. **2**, 013103 (2020).

[63] A. Pal, L. Kusmierz, and S. Reuveni, Search with home returns provides advantage under high uncertainty, Phys. Rev. Res. **2**, 043174 (2020).

[64] R. K. Singh, R. Metzler, and T. Sandev, Resetting dynamics in a confining potential, J. Phys. A. **53**, 505003 (2020).

[65] V. Domazetoski, A. Maso-Puigdellosas, T. Sandev, V. Mendez, A. Iomin, and L. Kocarev, Stochastic resetting on comblike structures, Phys. Rev. Res. **2**, 033027 (2020).

[66] B. Besga, A. Bovon, A. Petrosyan, S. N. Majumdar, and S. Ciliberto, Optimal mean first-passage time for a Brownian searcher subjected to resetting: experimental and theoretical results, Phys. Rev. Res **2**, 032029(R) (2020).

[67] O. Tal-Friedman, A. Pal, A. Sekhon, S. Reuveni, and Y. Roichman, Experimental realization of diffusion with stochastic resetting, J. Phys. Chem. Lett. **11**, 7350 (2020).

[68] A. F. M. dos Santos, Comb model with non-static stochastic resetting and anomalous diffusion, Fractal Fract. **4**, 28 (2020).

[69] P. C. Bressloff, Queueing theory of search processes with stochastic resetting, Phys. Rev. E **102**, 032109 (2020).

[70] A. Miron and S. Reuveni, Diffusion with local resetting and exclusion, Phys. Rev. Res. **3**, L012023 (2021).

[71] V. Mendez, A. Maso-Puigdellosas, T. Sandev, and D. Campos, Continuous time random walks under Markovian resetting, Phys. Rev. E **103**, 022103 (2021).

[72] T. Sandev, V. Domazetoski, A. Iomin, and L. Kocarev, Diffusion-advection equations on a comb: resetting and random search, MDPI: Math. **9**, 221 (2021).

[73] D. Gupta, C. A. Plata, A. Kundu, and A. Pal, Stochastic resetting with stochastic returns using external trap, J. Phys. A **54**, 025003 (2021).

[74] C. Monthus, Large deviations at various levels for run-and-tumble processes with space-dependent velocities and space-dependent switching rates, arXiv:2103.08885.

[75] P. Singh and A. Pal, Extremal statistics for stochastic resetting systems, Phys. Rev. E **103**, 052119 (2021).

[76] F. Mori, S. N. Majumdar, and G. Schehr, Detecting nonequilibrium dynamics via extreme value statistics, arXiv:2104.07346.

[77] M. Dahlenburg, A. V. Chechkin, R. Schumer, and R. Metzler, Stochastic resetting by a random amplitude, Phys. Rev. E **103**, 052123 (2021).

[78] F. H. Gonzalez, A. P. Riascos, and D. Boyer, Diffusive transport on networks with stochastic resetting to multiple nodes, Phys. Rev. E **103**, 062126 (2021).

[79] S. Ciliberto, Experiments in Stochastic Thermodynamics: Short History and Perspectives, Phys. Rev. X **7**, 021051 (2017).

[80] D. W. Stephens and J. R. Krebs, *Foraging Theory* (Princeton University Press, Princeton, NJ, 1986), Vol. 1.

[81] G. M. Viswanathan, S. V. Buldyrev, S. Havlin, M. G. E. da Luz, E. P. Raposo, and H. E. Stanley, Optimizing the success of random searches, Nature (London) **401**, 911 (1999).

[82] F. Bartumeus and J. Catalan, Optimal search behavior and classic foraging theory, J. Phys. A **42**, 434002 (2009).

[83] N. E. Humphries, H. Weimerskirch, N. Queiroz, E. J. Southall, and D. W. Sims, Foraging success of biological Lévy flights recorded *in situ*, Proc. Natl. Acad. Sci. USA **109**, 7169 (2012).

[84] T. H. Harris *et al.*, Generalized Lévy walks and the role of chemokines in migration of effector $CD8^+$ 1 T cells, Nature (London) **486**, 545 (2012).

[85] G. Ariel, A. Rabani, S. Benisty, J. D. Partridge, R. M. Harshey, and A. Be'er, Swarming bacteria migrate by Lévy walk, Nature Comm. **6**, 8396 (2015).

[86] T. Shokaku, T. Moriyama, H. Murakami, S. Shinohara, N. Manome, and K. Morioka, Development of an automatic turntable-type multiple T-maze device and observation of pill bug behavior, Rev. Sci. Instrum. **91**, 104104 (2020).

[87] B. Guinard and A. Korman, Intermittent inverse-square Lévy walks are optimal for finding targets of all sizes, Science Adv. **7**, eabe8211 (2021).

[88] W. Bell, *The Behavioural Ecology of Finding Resources* (Springer, Netherlands, 1990).

[89] P. Turchin, *Quantitative Analysis of Movement* (Sinauer Associates, Sunderland, MA, 1998).

[90] G. M. Viswanathan, M. G. E. da Luz, E. P. Raposo, and H. E. Stanley, *The Physics of Foraging: An Introduction to Random Searches and Biological Encounters* (Cambridge University Press, Cambridge, UK, 2011).

[91] O. Benichou, C. Loverdo, M. Moreau, and R. Voituriez, Intermittent search strategies, Rev. Mod. Phys. **83**, 81 (2011).

[92] R. Nathan *et al.*, A movement ecology paradigm for unifying organismal movement research, Proc. Natl. Acad. Sci. USA **105**, 19052 (2008).

[93] W. F. Fagan *et al.*, Spatial memory and animal movement, Ecology Lett. **16**, 1316 (2013).

[94] S. Benhamou, Of scales and stationarity in animal movements, Ecology Lett. **17**, 261 (2014).

[95] V. M. Kenkre and L. Giuggioli, *Theory of the Spread of Epidemics and Movement Ecology of Animals* (Cambridge University Press, Cambridge, UK, 2021).

[96] O. Vilk, Y. Orchan, M. Charter, N. Ganot, S. Toledo, R. Nathan, and M. Assaf, Ergodicity breaking and lack of a typical waiting time in area-restricted search of avian predators, arXiv:2101.11527.

[97] M. Slutsky, M. Kardar, and L. A. Mirny, Diffusion in correlated random potentials, with applications to DNA, Phys. Rev. E. **69**, 061903 (2004).

[98] M. Slutsky and L. A. Mirny, Kinetics of protein-DNA interaction: Facilitated target location in sequence-dependent potential, Biophys. J. **87**, 4021 (2004).

[99] I. M. Sokolov, R. Metzler, K. Pant, and M. C. Williams, Target search of N sliding proteins on a DNA, Biophys J. **89**, 895 (2005).

[100] A. G. Cherstvy, A. A. Kolomeisky, and A. A. Kornyshev, Protein-DNA interactions: Reaching and recognizing the targets, J. Phys. Chem. B **112**, 4741 (2008).

[101] A. B. Kolomeisky, Physics of protein-DNA interactions: Mechanisms of facilitated target search, Phys. Chem. Chem. Phys. **13**, 2088 (2011).

[102] E. Kussell, and S. Leibler, Phenotypic diversity, population growth, and information in fluctuating environments, Science **309**, 2075 (2005).

[103] N. Q. Balaban, J. Merrin, R. Chait, L. Kowalik, and S. Leibler, Bacterial persistence as a phenotypic switch, Science **305**, 1622 (2004).

[104] E. Kussell, R. Kishony, N. Q. Balaban, and S. Leibler, Bacterial persistence: A model of survival in changing environments, Genetics **169**, 1807 (2005).

[105] P. Visco, R. J. Allen, S. N. Majumdar, and M. R. Evans, Switching and growth for microbial populations in catastrophic responsive environments, Biophys. J. **98**, 1099 (2010).

[106] P. C. Bressloff, Stochastic switching in biology: From genotype to phenotype, J. Phys. A **50**, 133001 (2017).

[107] A. Taitelbaum, R. West, M. Assaf, and M. Mobilia, Population Dynamics in a Changing Environment: Random Versus Periodic Switching, Phys. Rev. Lett. **125**, 048105 (2020).

[108] M. L. Ginsberg, Dynamic backtracking, J. Artif. Intell. Res. **1**, 25 (1993).

[109] M. Luby, A. Sinclair, and D. Zuckerman, Optimal speedup of Las Vegas algorithms, Inf. Process. Lett. **47**, 173 (1993).

[110] C. P. Gomes, B. Selman, and H. Kautz, Boosting combinatorial search through randomization, Computer Sci. AAAI/IAAI **98**, 431 (1998).

[111] G. T. Buswell, *How People Look at Pictures: A Study of the Psychology And Perception in Art*, (Chicago University Press, 1935).

[112] D. Noton and L. Stark, Scanpaths in saccadic eye movements while viewing and recognizing patterns, Vision Res. **11**, 929 (1971).

[113] K. Rayner, Eye movements in reading and information processing, Psychol. Bull. **85**, 618 (1978).

[114] K. Rayner, Eye movements in reading and information processing: 20 years of research, Psychol. Bulletin **124**, 372 (1998).

[115] P. Verghese, Visual search and attention: A signal detection theory approach, Neuron **31**, 523 (2001).
[116] R. Engbert and R. Kliegl, Microsaccades uncover the orientation of covert attention, Vision Res. **43**, 1035 (2003).
[117] M. Rolfs, Microsaccades: small steps on a long way, Vision Res. **49**, 2415 (2009).
[118] R. Engbert, K. Mergenthaler, P. Sinn, and A. Pikovsky, An integrated model of fixational eye movements and microsaccades, Proc. Natl. Acad. Sci. USA **108**, E765 (2011).
[119] D. G. Stephen, D. Mirman, J. S. Magnuson, and J. A. Dixon, Lévy-like diffusion in eye movements during spoken-language comprehension, Phys. Rev. E **79**, 056114 (2009).
[120] C. J. J. Herrmann, R. Metzler, and R. Engbert, A self-avoiding walk with neural delays as a model of fixational eye movements, Sci. Rep. **7**, 12958 (2017).
[121] P. Blazejczyk and M. Magdziarz, Stochastic modeling of Lévy-like human eye movements, Chaos **31**, 043129 (2021).
[122] M. P. Eckstein, Visual search: A retrospective, J. Vision **11**, 14 (2011).
[123] A. Conze and Viswanathan, Path dependent options: The case of lookback options, J. Finance **XLVI**, 1893 (1991).
[124] M. Rubinstein and E. Reiner, Breaking down the barriers, Risk **4**, 28 (1991).
[125] S. F. Gray and R. E. Whaley, Valuing S&P 500 bear market warrants with a periodic reset, J. Deriv. **5**, 99 (1997).
[126] W.-Y. Cheng and S. Zhang, The analytics of reset options, J. Deriv. **8**, 59 (2000).
[127] D. Davydov and V. Linetsky, Pricing and hedging path-dependent options under the CEV process, Manag. Sci. **47**, 949 (2001).
[128] R. Goerlich, M. Li, S. Albert, G. Manfredi, P.-A. Hervieux, and C. Genet, Noise and ergodic properties of Brownian motion in an optical tweezer: Looking at the crossover between Wiener and Ornstein-Uhlenbeck processes, Phys. Rev. E **103**, 032132 (2021).
[129] S. C. Lim and S. V. Muniandy, Self-similar Gaussian processes for modeling anomalous diffusion, Phys. Rev. E **66**, 021114 (2002).
[130] F. Thiel and I. M. Sokolov, Scaled Brownian motion as a mean-field model for continuous-time random walks, Phys. Rev. E **89**, 012115 (2014).
[131] J.-H. Jeon, A. V. Chechkin, and R. Metzler, Scaled Brownian motion: A paradoxical process with a time dependent diffusivity for the description of anomalous diffusion, Phys. Chem. Chem. Phys. **16**, 15811 (2014).
[132] A. G. Cherstvy and R. Metzler, Ergodicity breaking, ageing, and confinement in generalized diffusion processes with position and time dependent diffusivity, J. Stat. Mech. (2015) P05010.
[133] A. Bodrova, A. V. Chechkin, A. G. Cherstvy, and R. Metzler, Ultraslow scaled Brownian motion, New J. Phys. **17**, 063038 (2015).
[134] H. Safdari, A. G. Cherstvy, A. V. Chechkin, F. Thiel, I. M. Sokolov, and R. Metzler, Quantifying the non-ergodicity of scaled Brownian motion, J. Phys. A **48**, 375002 (2015).
[135] A. G. Cherstvy, and R. Metzler, Anomalous diffusion in time-fluctuating non-stationary diffusivity landscapes, Phys. Chem. Chem. Phys. **18**, 23840 (2016).
[136] H. Safdari, A. G. Cherstvy, A. V. Chechkin, A. Bodrova, and R. Metzler, Aging underdamped scaled Brownian motion: Ensemble- and time-averaged particle displacements, nonergodicity, and the failure of the overdamping approximation, Phys. Rev. E **95**, 012120 (2017).
[137] A. G. Cherstvy, H. Safdari, and R. Metzler, Anomalous diffusion, nonergodicity, and ageing for exponentially and logarithmically time-dependent diffusivity: Striking differences for massive versus massless particles, J. Phys. D **54**, 195401 (2021).
[138] J. L. Lebowitz and O. Penrose, Modern ergodic theory, Phys. Today **26**(2), 23 (1973).
[139] J.-P. Bouchaud, Weak ergodicity breaking and aging in disordered systems, J. Phys. I **2**, 1705 (1992).
[140] C. C. Moore, Ergodic theorem, ergodic theory, and statistical mechanics, Proc. Natl. Acad. Sci. USA **112**, 1907 (2015).
[141] M. Mangalam and D. G. Kelty-Stephen, Point estimates, Simpson's paradox, and nonergodicity in biological sciences, Neurosci. Biobehav. Rev. **125**, 98 (2021).
[142] A. N. Kolmogorov, Wienersche Spiralen und einige andere interessante Kurven im Hilbertschen Raum, C. R. (Doklady) Acad. Sci. URSS (N.S.) **26**, 115 (1940).
[143] B. B. Mandelbrot and J. W. van Ness, Fractional Brownian motions, fractional noises and applications, SIAM Rev. **10**, 422 (1968).
[144] F. Biagini, Y. Hu, B. Øksendal, and T. Zhang, *Stochastic Calculus for Fractional Brownian Motion and Applications* (Springer-Verlag, London, 2008).
[145] W. Deng and E. Barkai, Ergodic properties of fractional Brownian-Langevin motion, Phys. Rev. E **79**, 011112 (2009).
[146] J.-H. Jeon and R. Metzler, Fractional Brownian motion and motion governed by the fractional Langevin equation in confined geometries, Phys. Rev. E **81**, 021103 (2010).
[147] J.-H. Jeon and R. Metzler, Inequivalence of time and ensemble averages in ergodic systems: Exponential versus power-law relaxation in confinement, Phys. Rev. E **85**, 021147 (2012).
[148] F. Thiel and I. M. Sokolov, Weak ergodicity breaking in an anomalous diffusion process of mixed origins, Phys. Rev. E **89**, 012136 (2014).
[149] M. Schwarzl, A. Godec, and R. Metzler, Quantifying nonergodicity of anomalous diffusion with higher order moments, Sci. Rep. **7**, 3878 (2017).
[150] W. Wang, A. G. Cherstvy, A. V. Chechkin, S. Thapa, F. Seno, X. Liu, and R. Metzler, Fractional Brownian motion with random diffusivity: Emerging residual nonergodicity below the correlation time, J. Phys. A **53**, 474001 (2020).
[151] A. G. Cherstvy, A. V. Chechkin, and R. Metzler, Anomalous diffusion and ergodicity breaking in heterogeneous diffusion processes, New J. Phys. **15**, 083039 (2013).
[152] A. G. Cherstvy and R. Metzler, Nonergodicity, fluctuations, and criticality in heterogeneous diffusion processes, Phys. Rev. E **90**, 012134 (2014).
[153] A. G. Cherstvy, A. V. Chechkin, and R. Metzler, Ageing and confinement in non-ergodic heterogeneous diffusion processes, J. Phys. A **47**, 485002 (2014).
[154] A. G. Cherstvy and R. Metzler, Ergodicity breaking and particle spreading in noisy heterogeneous diffusion processes, J. Chem. Phys. **142**, 144105 (2015).

[155] W. Wang, A. G. Cherstvy, X. Liu, and R. Metzler, Anomalous diffusion and nonergodicity for heterogeneous diffusion processes with fractional Gaussian noise, Phys. Rev. E **102**, 012146 (2020).

[156] H. Hurst, Long term storage capacity of reservoirs, Trans. Am. Soc. Civil Eng. **116**, 770 (1951).

[157] B. B. Mandelbrot, *Harold Edwin Hurst*, in Statisticians of the Centuries, edited by C. C. Heyde (Springer, New York, 2001).

[158] J. E. Higham, M. Shahnam, and A. Vaidheeswaran, Anomalous diffusion in a bench-scale pulsed fluidized bed, Phys. Rev. E **103**, 043103 (2021).

[159] Y. He, S. Burov, R. Metzler, and E. Barkai, Random Time-Scale Invariant Diffusion and Transport Coefficients, Phys. Rev. Lett. **101**, 058101 (2008).

[160] A. W. C. Lau and T. C. Lubensky, State-dependent diffusion: Thermodynamic consistency and its path integral formulation, Phys. Rev. E **76**, 011123 (2007).

[161] J.-H. Jeon, H. Martinez-Seara Monne, M. Javanainen, and R. Metzler, Anomalous Diffusion of Phospholipids and Cholesterols in a Lipid Bilayer and Its Origins, Phys. Rev. Lett. **109**, 188103 (2012).

[162] J.-H. Jeon, M. Javanainen, H. Martinez-Seara, R. Metzler, and I. Vattulainen, Protein Crowding in Lipid Bilayers Gives Rise to Non-Gaussian Anomalous Lateral Diffusion of Phospholipids and Proteins, Phys. Rev. X **6**, 021006 (2016).

[163] R. Metzler, J.-H. Jeon, and A. G. Cherstvy, Non-Brownian diffusion in lipid membranes: Experiments and simulations, Biochem. Biophys. Acta BBA-Biomembr. **1858**, 2451 (2016).

[164] Y. Golan and E. Sherman, Resolving mixed mechanisms of protein subdiffusion at the T cell plasma membrane, Nature Comm. **8**, 15851 (2017)

[165] T. Sungkaworn, M.-L. Jobin, K. Burnecki, A. Weron, M. J. Lohse, and D. Calebiro, Single-molecule imaging reveals receptor-G protein interactions at cell surface hot spots, Nature (London) **550**, 543 (2017).

[166] J. Janczura, P. Kowalek, H. Loch-Olszewska, J. Szwabinski, and A. Weron, Classification of particle trajectories in living cells: Machine learning versus statistical testing hypothesis for fractional anomalous diffusion, Phys. Rev. E **102**, 032402 (2020).

[167] M. Magdziarz, A. Weron, K. Burnecki, and J. Klafter, Fractional Brownian Motion Versus the Continuous-Time Random Walk: A Simple Test for Subdiffusive Dynamics, Phys. Rev. Lett. **103**, 180602 (2009).

[168] J.-H. Jeon, V. Tejedor, S. Burov, E. Barkai, C. Selhuber-Unkel, K. Berg-Sørensen, L. Oddershede, and R. Metzler, *In vivo* Anomalous Diffusion and Weak Ergodicity Breaking of Lipid Granules, Phys. Rev. Lett. **106**, 048103 (2011).

[169] E. Kepten, I. Bronshtein, and Y. Garini, Ergodicity convergence test suggests telomere motion obeys fractional dynamics, Phys. Rev. E **83**, 041919 (2011).

[170] K. Burnecki, E. Kepten, J. Janczura, I. Bronshtein, Y. Garini, and A. Weron, Universal algorithm for identification of fractional Brownian motion. A case of telomere subdiffusion, Biophys. J. **103**, 1839 (2012).

[171] S. C. Weber, M. A. Thompson, W. E. Moerner, A. J. Spakowitz, and J. A. Theriot, Analytical tools to distinguish the effects of localization error, confinement, and medium elasticity on the velocity autocorrelation function, Biophys. J. **102**, 2443 (2012).

[172] M. P. Backlund, R. Joyner, and W. E. Moerner, Chromosomal locus tracking with proper accounting of static and dynamic errors, Phys. Rev. E **91**, 062716 (2015).

[173] G. M. Oliveira, A. Oravecz, D. Kobi, M. Maroquenne, K. Bystricky, T. Sexton, and N. Molina, Precise measurements of chromatin diffusion dynamics by modeling using Gaussian processes, bioRxiv: https://doi.org/10.1101/2021.03.16.435699 (2021).

[174] A. G. Cherstvy, S. Thapa, C. E. Wagner, and R. Metzler, Non-Gaussian, non-ergodic, and non-Fickian diffusion of tracers in mucin hydrogels, Soft Matter **15**, 2526 (2019).

[175] I. Y. Wong, M. L. Gardel, D. R. Reichman, E. R. Weeks, M. T. Valentine, A. R. Bausch, and D. A. Weitz, Anomalous Diffusion Probes Microstructure Dynamics of Entangled F-Actin Networks, Phys. Rev. Lett. **92**, 178101 (2004).

[176] M. Levin, G. Bel, and Y. Roichman, Measurements and characterization of the dynamics of tracer particles in an actin network, J. Chem. Phys. **154**, 144901 (2021).

[177] A. Muralidharan, H. Uitenbroek, and P. E. Boukany, Intracellular transport of electro-transferred DNA cargo is governed by coexisting ergodic and nonergodic anomalous diffusion, bioRxiv: https://doi.org/10.1101/2021.04.12.435513

[178] A. D. Fernandez, P. Charchar, A. G. Cherstvy, R. Metzler, and M. F. Finnis, The diffusion of doxorubicin drug molecules in silica nanoslits is non-Gaussian, intermittent and anticorrelated, Phys. Chem. Chem. Phys. **22**, 27955 (2020).

[179] R. Benelli and M. Weiss, From sub- to superdiffusion: fractional Brownian motion of membraneless organelles in early *C. elegans* embryos, New J. Phys. **23**, 063072 (2021).

[180] S. M. J. Khadem, S. H. L. Klapp, and R. Klages, Search efficiency of discrete fractional Brownian motion in a random distribution of targets, Phys. Rev. Res. **3**, 023169 (2021).

[181] L. Boltzmann, Zur Integration der Diffusionsgleichung bei variabeln Diffusionscoefficienten, Ann. Physik **289**, 959 (1894).

[182] R. E. Pattle, Diffusion from an instantaneous point source with a concentration-dependent coefficient, Q. J. Mech. Appl. Math. **12**, 407 (1959).

[183] A. Hansen, E. G. Flekkøy, and B. Baldelli, Anomalous diffusion in systems with concentration-dependent diffusivity: Exact solutions and particle simulations, Front. Phys. **8**, 519624 (2020).

[184] A. Hansen, E. G. Flekkøy, and B. Baldelli, Hyperballistic superdiffusion and explosive solutions to the non-linear diffusion equation, Front. Phys. **9**, 640560 (2021).

[185] A. Fulinski, Communication: How to generate and measure anomalous diffusion in simple systems, J. Chem. Phys. **138**, 021101 (2013).

[186] M. Heidernätsch, diffusion in inhomogeneous systems, Ph.D. thesis, TU Chemnitz, 2015.

[187] R. Kazakevicius and J. Ruseckas, Influence of external potentials on heterogeneous diffusion processes, Phys. Rev. E **94**, 032109 (2016).

[188] X. Wang, W. Deng, and Y. Chen, Ergodic properties of heterogeneous diffusion processes in a potential well, J. Chem. Phys. **150**, 164121 (2019).

[189] M. A. F. dos Santos, V. Dornelas, E. H. Colombo, and C. Anteneodo, Critical patch size reduction by heterogeneous diffusion, Phys. Rev. E **102**, 042139 (2020).

[190] T. Sandev, A. Schulz, H. Kantz, and A. Iomin, Heterogeneous diffusion in comb and fractal grid structures, Chaos Solitons Fractals **114**, 551 (2018).
[191] N. Leibovich and E. Barkai, Infinite ergodic theory for heterogeneous diffusion processes, Phys. Rev. E **99**, 042138 (2019).
[192] R. Kazakevicius and A. Kononovicius, Anomalous diffusion in nonlinear transformations of the noisy voter model, Phys. Rev. E **103**, 032154 (2021).
[193] S. K. Ghosh, A. G. Cherstvy, D. S. Grebenkov, and R. Metzler, Anomalous, non-Gaussian tracer diffusion in crowded two-dimensional environments, New J. Phys. **18**, 013027 (2016).
[194] P. Massignan, C. Manzo, J. A. Torreno-Pina, M. F. Garcia-Parajo, M. Lewenstein, and G. J. Lapeyre, Jr., Nonergodic Subdiffusion from Brownian Motion in an Inhomogeneous Medium, Phys. Rev. Lett. **112**, 150603 (2014).
[195] R. Jain and K. L. Sebastian, Diffusion in a crowded, rearranging environment, J. Phys. Chem. B **120**, 3988 (2016).
[196] H. Berry and H. Chate, Anomalous diffusion due to hindering by mobile obstacles undergoing Brownian motion or Ornstein-Uhlenbeck processes, Phys. Rev. E **89**, 022708 (2014).
[197] F. Trovato and V. Tozzini, Diffusion within the cytoplasm: a mesoscale model of interacting macromolecules, Biophys. J. **107**, 2579 (2014).
[198] M. Weiss, Crowding, diffusion, and biochemical reactions, Intl. Rev. Cell Mol. Biol. **307**, 383 (2014).
[199] M. J. Saxton, Wanted: scalable tracers for diffusion measurements, J. Phys. Chem. B **118**, 12805 (2014).
[200] A. Russian, M. Dentz, and P. Gouze, Self-averaging and weak ergodicity breaking of diffusion in heterogeneous media, Phys. Rev. E **96**, 022156 (2017).
[201] Y. Lanoiselee, N. Moutal, D. S. Grebenkov, Diffusion-limited reactions in dynamic heterogeneous media, Nature Comm. **9**, 4398 (2018).
[202] S. Basak, S. Sengupta, and K. Chattopadhyay, Understanding biochemical processes in the presence of sub-diffusive behavior of biomolecules in solution and living cells, Biophys. Rev. **11**, 851 (2019).
[203] P. Witzel, M. Götz, Y. Lanoiselee, T. Franosch, D. S. Grebenkov, and D. Heinrich, Heterogeneities shape passive intracellular transport, Biophys. J. **117**, 203 (2019).
[204] G. Munoz-Gil, M. A. Garcia-March, C. Manzo, A. Celi, and M. Lewenstein, Diffusion through a network of compartments separated by partially transmitting boundaries, Front. Phys. **7**, 31 (2019).
[205] A. Sabri, X. Xu, D. Krapf, and M. Weiss, Elucidating the Origin of Heterogeneous Anomalous Diffusion in the Cytoplasm of Mammalian Cells, Phys. Rev. Lett. **125**, 058101 (2020).
[206] I. Chakraborty and Y. Roichman, Disorder-induced Fickian, yet non-Gaussian diffusion in heterogeneous media, Phys. Rev. Res. **2**, 022020(R) (2020).
[207] E. B. Postnikov, A. V. Chechkin, and I. M. Sokolov, Brownian yet non-Gaussian diffusion in heterogeneous media: From superstatistics to homogenization, New J. Phys. **22**, 063046 (2020).
[208] M. J. Skaug and D. K. Schwartz, Tracking nanoparticle diffusion in porous filtration media, Ind. Eng. Chem. Res. **54**, 4414 (2015).
[209] M. J. Skaug, L. Wang, Y. Ding, and D. K. Schwartz, Hindered nanoparticle diffusion and void accessibility in a three-dimensional porous medium, ACS Nano **9**, 2148 (2015).
[210] R. Sarfati, C. P. Calderon, and D. K. Schwartz, Enhanced diffusive transport in fluctuating porous media, ACS Nano **15**, 7392 (2021).
[211] C. B. Mast, S. Schink, U. Gerland, and D. Braun, Escalation of polymerization in a thermal gradient, Proc. Natl. Acad. Sci. USA **110**, 8030 (2013).
[212] D. Breoni, H. Löwen, and R. Blossey, Active noise-driven particles under space-dependent friction in one dimension, Phys. Rev. E **103**, 052602 (2021).
[213] P. Massignan, A. Lampo, J. Wehr, and M. Lewenstein, Quantum Brownian motion with inhomogeneous damping and diffusion, Phys. Rev. A **91**, 033627 (2015)
[214] N. Korabel, D. Han, A. Taloni, G. Pagnini, S. Fedotov, V. Allan, and T. A. Waigh, Local analysis of heterogeneous intracellular transport: slow and fast moving endosomes, Entropy **23**, 958 (2021).
[215] J. Crank, *The Mathematics of Diffusion* (Oxford University Press, Oxford, UK, 1975).
[216] W. S. Gurney and R. M. Nisbet, The regulation of inhomogeneous populations, J. Theor. Biol. **52**, 441 (1975).
[217] M. E. Gurtin and R. C. MacCamy, On the diffusion of biological populations, Math. Biosci. **33**, 35 (1977).
[218] W. I. Newman, Some exact solutions to a non-linear diffusion problem in population genetics and combustion, J. Theor. Biol. **85**, 325 (1980).
[219] D. G. Aronson, The porous medium equation, in *Nonlinear Diffusion Problems*, in Lecture Notes in Mathematics, edited by A. Dold and B. Eckmann (Springer-Verlag, Berlin, 1986), Vol. 1224, pp. 1–46.
[220] I. C. Christov and H. A. Stone, Resolving a paradox of anomalous scalings in the diffusion of granular materials, Proc. Natl. Acad. Sci. USA **109**, 16012 (2012).
[221] A. G. Cherstvy, S. Thapa, Y. Mardoukhi, A. V. Chechkin, and R. Metzler, Time averages and their statistical variation for the Ornstein-Uhlenbeck process: Role of initial particle conditions and relaxation to stationarity, Phys. Rev. E **98**, 022134 (2018).
[222] G. E. Uhlenbeck and L. S. Ornstein, On the theory of the Brownian motion, Phys. Rev. **36**, 823 (1930).
[223] W. Wang *et al.*, Nonergodicity of reset fractional Brownian motion (unpublished).
[224] Metaphorically, after Henri de Pitot (also known as "satellite droplet(s)"), see, e.g., Ya. E. Gegusin, *The Drop* (Moscow, Nauka, 1973) [in Russian].
[225] B. Goswami, N. Boers, A. Rheinwalt, N. Marwan, J. Heitzig, S. F. M. Breitenbach, and J. Kurths, Abrupt transitions in time series with uncertainties, Nature Comm. **9**, 48 (2018).
[226] R. Hou, A. G. Cherstvy, R. Metzler, and T. Akimoto, Biased continuous-time random walks for ordinary and equilibrium cases: Facilitation of diffusion, ergodicity breaking and ageing, Phys. Chem. Chem. Phys. **20**, 20827 (2018).
[227] V. Zaburdaev, S. Denisov, and J. Klafter, Lévy walks, Rev. Mod. Phys. **87**, 483 (2015).
[228] A. G. Cherstvy, D. Vinod, E. Aghion, A. V. Chechkin, and R. Metzler, Time averaging, ageing and delay analysis of financial time series, New J. Phys. **19**, 063045 (2017).

[229] S. Ritschel, A. G. Cherstvy, and R. Metzler, Universality of delay-time averages for financial time series: Analytical results, computer simulations, and analysis of historical stock-market prices (unpublished).

[230] D. Vinod, A. G. Cherstvy, W. Wang, I. M. Sokolov, and R. Metzler, Resetting, time-averaging, and nonergodicity for geometric Brownian motion (unpublished).

[231] A. G. Cherstvy, D. Vinod, E. Aghion, I. M. Sokolov, and R. Metzler, Scaled geometric Brownian motion features sub- or superexponential ensemble- but linear time-averaged mean-squared displacements, Phys. Rev. E **103**, 062127 (2021).

[232] V. Stojkoski, T. Sandev, L. Kocarev, and A. Pal, Geometric Brownian motion under stochastic resetting: A stationary yet non-ergodic process, Phys. Rev. E **104**, 014121 (2021).

[233] S. Petrovskii and A. Morozov, Dispersal in a statistically structured population: Fat tails revisited, Am. Naturalist **173**, 278 (2009).

[234] S. Hapca, J. W. Crawford, and L. M. Young, Anomalous diffusion of heterogeneous populations characterized by normal diffusion at the individual level, J. Royal Soc. Interface **6**, 111 (2009).

[235] M. V. Chubynsky and G. W. Slater, Diffusing Diffusivity: A Model for Anomalous, Yet Brownian, Diffusion, Phys. Rev. Lett. **113**, 098302 (2014).

[236] T. Uneyama, T. Miyaguchi, and T. Akimoto, Fluctuation analysis of time-averaged mean-square displacement for the Langevin equation with time-dependent and fluctuating diffusivity, Phys. Rev. E **92**, 032140 (2015).

[237] A. V. Chechkin, F. Seno, R. Metzler, and I. M. Sokolov, Brownian Yet Non-Gaussian Diffusion: From Superstatistics to Subordination of Diffusing Diffusivities, Phys. Rev. X **7**, 021002 (2017).

[238] R. Jain and K. L. Sebastian, Lévy flight with absorption: A model for diffusing diffusivity with long tails, Phys. Rev. E **95**, 032135 (2017).

[239] A. Weron, K. Burnecki, E. J. Akin, L. Sole, M. Balcerek, M. M. Tamkun, and D. Krapf, Ergodicity breaking on the neuronal surface emerges from random switching between diffusive states, Sci. Rep. **7**, 5404 (2017).

[240] T. Miyaguchi, T. Uneyama, and T. Akimoto, Brownian motion with alternately fluctuating diffusivity: Stretched-exponential and power-law relaxation, Phys. Rev. E **100**, 012116 (2019).

[241] M. A. F. dos Santos, E. H. Colombo, and C. Anteneodo, Random diffusivity scenarios behind anomalous non-Gaussian diffusion, arXiv:2106.10525 (2021).

[242] D. S. Grebenkov, V. Sposini, R. Metzler, G. Oshanin, and F. Seno, Exact first-passage time distributions for three random diffusivity models, J. Phys. A **54**, 04LT01 (2021).

[243] V. Sposini, D. S. Grebenkov, R. Metzler, G. Oshanin, and F. Seno, Universal spectral features of different classes of random-diffusivity processes, New J. Phys. **22**, 063056 (2020).